Tampere University

Mikko Hongisto

ADVANCED PARTICLE CONTAINING GLASSES FOR PHOTONICS

ABSTRACT

Mikko Hongisto: Advanced particle containing glasses for photonics
Master's Thesis
Tampere University
Master's degree program in Science and Engineering
August 2019

This work studied different techniques to prepare particle containing phosphate glasses. Additionally, a process to sinter these glasses by hot uniaxial pressing was studied and developed. Our goal was to prepare and to create transparent, particle containing glasses for photonic applications. So far, the challenge has been to prepare these glasses without significant agglomeration or corrosion of the particles during glass preparation.

Erbium and ytterbium containing YAG nanoparticles and erbium containing 75 NaPO3 - 25 CaF2 (mol-%) glass-ceramic microparticles were mixed in with 90 NaPO3 - 10 NaF (mol-%) phosphate glass raw materials and already molten phosphate glass. In addition to YAG and glass ceramic particles, erbium and ytterbium doped $NaYF_4$ particles were mixed with powdered glass and sintered into a solid glass. The effects of the sintering process on the particles were studied using commercial luminescent microparticles.

Parameters for the sintering process were optimized to produce transparent glass successfully. The produced glass is clearly transparent, but has a brown coloration to it. The source of the coloration is presumed to be either nanoscale defects scattering shorter wavelengths of light or carbon contamination. Luminescent particles survived the sintering process unchanged according to our luminescence measurements and therefore we presume the process to be safe for other particles as well.

YAG agglomerates were visible to the naked eye inside the glass when they were added in the glass batch. When added in the melt, the particles stayed on the top and did not diffuse inside the glass. According to emission measurements, the structure had changed in both cases. The glasses had an inhomogeneous distribution of particles and emission. The sintered glass had unchanged emission spectrum compared to the pure particles and a tenfold increase in emission intensity relative to other methods of preparation. The resulting glass was not transparent due to particle agglomeration.

Glass-ceramic particles did not survive the glass manufacturing or addition into the molten glass. Sintering glass-ceramic particles with the host glass produces a somewhat transparent glass, but with a narrower emission spectrum.

$NaYF_4$ particles containing glass was also transparent with an unchanged emission spectrum. The particles were agglomerated and the glass had crystallized at the glass-particle -interface.

Keywords: phosphate glass, sintering, laser glass, nanoparticles

The originality of this thesis has been checked using the Turnitin OriginalityCheck service.

TIIVISTELMÄ

Mikko Hongisto: Advanced particle containing glasses for photonics
Diplomityö
Tampereen yliopisto
Teknillis-luonnontieteellinen tutkinto-ohjelma
Elokuu 2019

Tässä työssä tutkittiin erilaisia tekniikoita partikkeleita sisältävän fosfaattilasien valmistamiseksi. Lisäksi tässä työssä tutkittiin ja kehitettiin prosessi lasin valmistamiseksi murskatusta ja jauhetusta fosfaattilasista sintraamalla uniaksiaalisella kuumaprässillä. Tavoitteena oli kehittää läpinäkyviä, partikkeleita sisältäviä laseja fotoniikan sovellutuksiin. Tähän asti haasteena ovat olleet partikkelien kasautuminen suuriksi agglomeraateiksi tai partikkelien hajoamien ja korroosio valmistuksen aikana.

Erbiumia ja ytterbiumia sisältäviä YAG -nanopartikkeleita sekä erbiumia sisältävää 75 $NaPO_3$ - 25 CaF_2 (mol-%) lasikeraamisia mikropartikkeleita lisättiin 90 $NaPO_3$ - 10 NaF (mol-%) fosfaattilasin raaka-aineiden joukkoon ja sulaan lasiin. YAG ja lasikeraamipartikkelien lisäksi erbiumia ja ytterbiumia sisältäviä $NaYF_4$ partikkeleita sekoitettiin lasijauheen joukkoon ja sintrattiin kokoon. Sintrausprosessin vaikutuksia tutkittiin kaupallisilla luminoivilla partikkeleilla.

Sintrausprosessin parametrit optimoitiin tuottamaan läpinäkyvää lasia, tässä onnistuen. Saatu lasi on selvästi läpinäkyvää, mutta ruskeata. Väritys johtunee joko nanokokoisista huokosista tai hiilikontaminaatiosta. Luminoivat partikkelit selvisivät luminesenssimittausten mukaan muuttumattomina sintrausprosessista, joten pystyimme olettamaan sintrausprosessin olevan turvallinen muillekin partikkeleille.

YAG-partikkelien agglomeraatteja oli nähtävissä valmiin lasin sisässä, kun partikkelit lisättiin raaka-aineiden joukkoon. Lisättäessä sulaan lasiin, partikkelit kerääntyivät pinnalle eivätkä diffusoituneet pidemmälle. Emissiomittausten mukaan partikkelien rakenne oli kuitenkin muuttunut molemmissa tapauksissa. Emissio oli myös alueellisesti epähomogeenista. Sintratussa lasissa emissiospektri oli muuttumaton pelkkiin partikkeleihin verrattuna ja intensiteetti kymmenkertainen muihin valmistustekniikkoihin verraten. Saatu lasi oli homogeenistä, muttei kuitenkaan läpinäkyvää johtuen partikkelien agglomeraatiosta.

Lasikeraamipartikkelit eivät selvinneet lasin valmistuksesta eivätkä lisäämisestä sulaan lasiin. Sintratessa saatiin läpinäkyvää lasia, mutta partikkelien emissiospektri kapeni merkittävästi, syytä tälle käytökselle ei kuitenkaan ole tiedossa.

$NaYF_4$ partikkeleita sisältävä sintrattu lasi oli myös läpinäkyvää ja emissiospektri muuttumaton. Partikkelit olivat kuitenkin agglomeroituneet, ja lasi oli kristallisoitunut partikkelien ja ympäröivän lasin rajapinnassa.

Avainsanat: fosfaattilasi, sintraus, laserlasi, nanopartikkelit

Tämän julkaisun alkuperäisyys on tarkastettu Turnitin OriginalityCheck –ohjelmalla.

PREFACE

I would like to thank my supervisors, Associate Professor Laeticia Petit and Post-Doctoral researcher Alexander Veber for their assistance, guidance and support during my work. I would also like to thank Turkka Salminen here at TUNI for his help with the SEM and Mika Lastusaari at Turku University for his persistent luminescent measurements. Finally, I would like to extend my thanks to the entire Photonics Glasses Group, for all the help received during this thesis.

Tampere, 28 August 2019

Mikko Hongisto

CONTENTS

LIST OF FIGURES

LIST OF SYMBOLS AND ABBREVIATIONS

h	Planck constant
$\hbar$	reduced Planck constant
M	molar mass
m	mass
n	molar amount
Q^n	Q-notation, n denotes number of linked oxygens
R	particle radius
r	radius of curvature for a bubble/pore
r^*	critical particle radius for nucleation
t	time
T	temperature
T_m	glass melting temperature
T_g	glass transition temperature
T_p	peak crystallization temperature
T_x	crystallization onset temperature
V_0	initial volume
x	fraction amount
ΔV	change in volume
ΔG^*	barrier energy for nucleation
ΔP	pressure difference at an interface
γ	surface tension
η	viscosity
ν	photon frequency
ρ	density
Ω	angular frequency of a phonon
ω_0	angular frequency of a photon

DSC	differential scanning calorimetry
EDS	energy dispersive x-ray spectroscopy
GC	glass-ceramic
mol-%	mole percent
PeL	persistent luminescence
RE	rare earth
SEM	scanning electron microscope
UV	ultraviolet
wt%	weight percent
XRD	x-ray diffraction
YAG	yttrium aluminum garnet

1. INTRODUCTION

Lasers and glasses are found in multitude of applications, from scientific applications, such as spectroscopy or laser fusion, to industrial and commercial applications, with cutting and welding being some important applications. Lasers together with optical glasses form the backbone of our connected society by transmitting vast amounts of data through optical fibers. Glasses are an important medium for lasers as rare-earth doped glasses provide great properties for various applications. [1, p.82]

Ever since the first glass lasers in 1961[1, p.106], researchers around the world have been studying and developing ways to improve glass lasers and their properties. Lately, research has been conducted towards incorporating active nanoscale particles into the bulk glass.[2-6] As the Rare-earth doped particles can be manufactured separately from the glass, their properties, especially their spectroscopic properties, could therefore be optimized independently of the glass composition leading to active glasses with improved performance.

Various methods have been tried around the world and in the Photonic glasses group at Tampere University. The simplest solution is to add the particles in with the starting material so that the glass melt is formed with the particles already inside. The problem with this method is that the particles must be extremely durable as the molten glass is a thermally and chemically corrosive environment.[6, 7] This approach therefore limits the available options for particle materials.

A method to reduce the corrosive behavior is to add the particles in the melt in a process known as direct doping. In direct doping, the particles are added into the already molten glass. This method reduces the corrosion of the particles. Studies have shown that the particles do survive the doping process, but homogeneity of the resulting glass leaves room for improvement.[3, 7]

A third option is to mix powdered glass and the particles and to sinter the compact into a transparent solid. This process has been tried on fluorescent microparticles [8]. However the hot-sintering technique requires precise control of many parameters (time, temperature, pressure, particles size etc.), which are different for various glasses and dopant particles. Therefore, the method requires thorough investigation and optimization for every new glass-ceramic composition.

The purpose of this thesis is to synthetize and compare novel phosphate based glass-ceramics materials obtained using different techniques: by adding the particles in the glass batch and in the melt as well as the hot-sintering process. Special attention is paid to the corrosion and degradation of particles during different synthesis methods, homogeneity of the particles dispersion in the final glass-ceramics, optical, in particular luminescence, properties of the obtained glass-ceramic. Significant part of the work is dedicated to optimization of the glass sintering process in order to prepare particles containing glasses with homogeneous dispersion of a large amount of particles. This thesis will also set the groundwork for sintering experiments and research in our quest to achieve ever-greater performance out of our lasers.

Chapter 2 explains the basics of glasses and rare-earth elements. This chapter will also describe the basic physical processes encountered in laser light generation. The current methods of achieving crystal containing glasses are explained in more detail, along with current state of the art. Basic physics of sintering glasses is reviewed to see which parameters affect the process and should be noted in experiments.

Chapter 3 describes the different glasses prepared for this study, along with the precursors and processes used. The particles that are to be added to glass are also introduced. The process parameters are given for different methods of preparation. The equipment used to characterize the glasses and their working principles are detailed in brief.

Chapter 4 explains first the experimental process that is used to optimize the sintering parameters. The impact of the sintering process on the survival of the particles was investigated using commercial luminescent microparticles before moving to laser active materials. Finally, we present the spectroscopic properties of various particle containing glasses prepared using different techniques in order to define which technique should be used in order to prepare a glass which possess, homogeneously within the volume, the spectroscopic properties of the particles.

Chapter 5 concludes the thesis with summarizing remarks. Possible further studies are discussed with recommendations for future improvements.

2. BACKGROUND

2.1 Glasses

2.1.1 Definition of glasses

To date, all glasses share so far two common features. First, glasses lack a long range, periodic structure commonly found in crystalline materials. While the neighboring atoms may be the same throughout the material, bond angles and lengths are not the same, leading to an amorphous solid. Figure 1 shows a schematic comparison of the atomic arrangement between crystalline material (a) and amorphous glass (b).
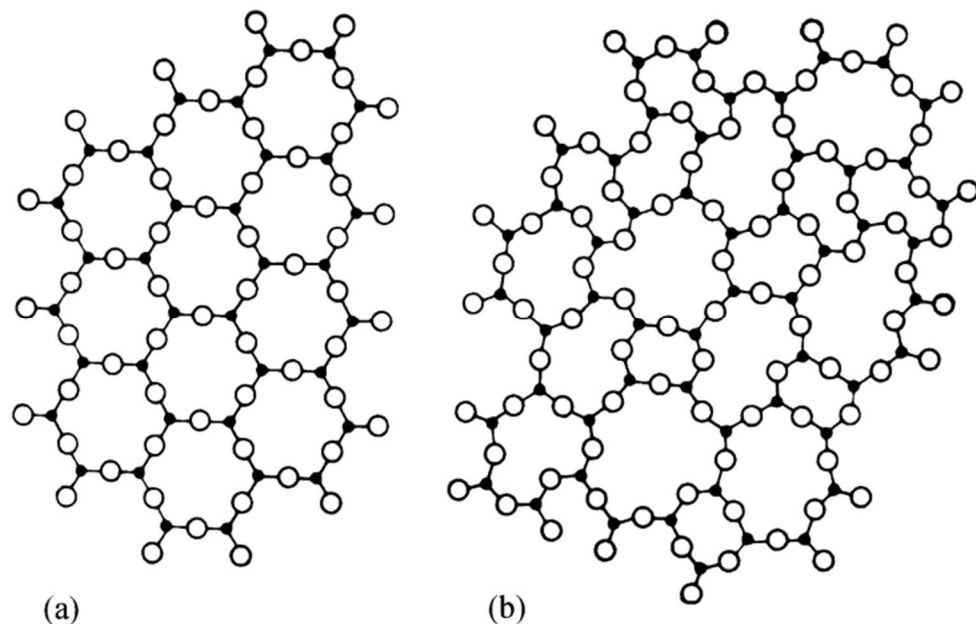
Figure 1. Schematic two-dimensional illustration of atomic arrangement in crystal (a) and glass (b). [9] as cited in[1, p.2]

The crystalline material shows distinct periodicity, whereas the amorphous arrangement can be seen as a deformed version of the crystalline materials. Both arrangements have the same neighboring atoms, only the structure is different.

Second, all glasses exhibit time-dependent glass transformation behavior. Glass transformation is the property of molten glass, from supercooled liquid to a solid without undergoing crystallization. The exponential increase in viscosity during cooling "locks in" the glass structure, preventing the formation of crystals. [10, p.3] The glass transition behavior can be demonstrated on a temperature-enthalpy curve, shown in Figure 2.
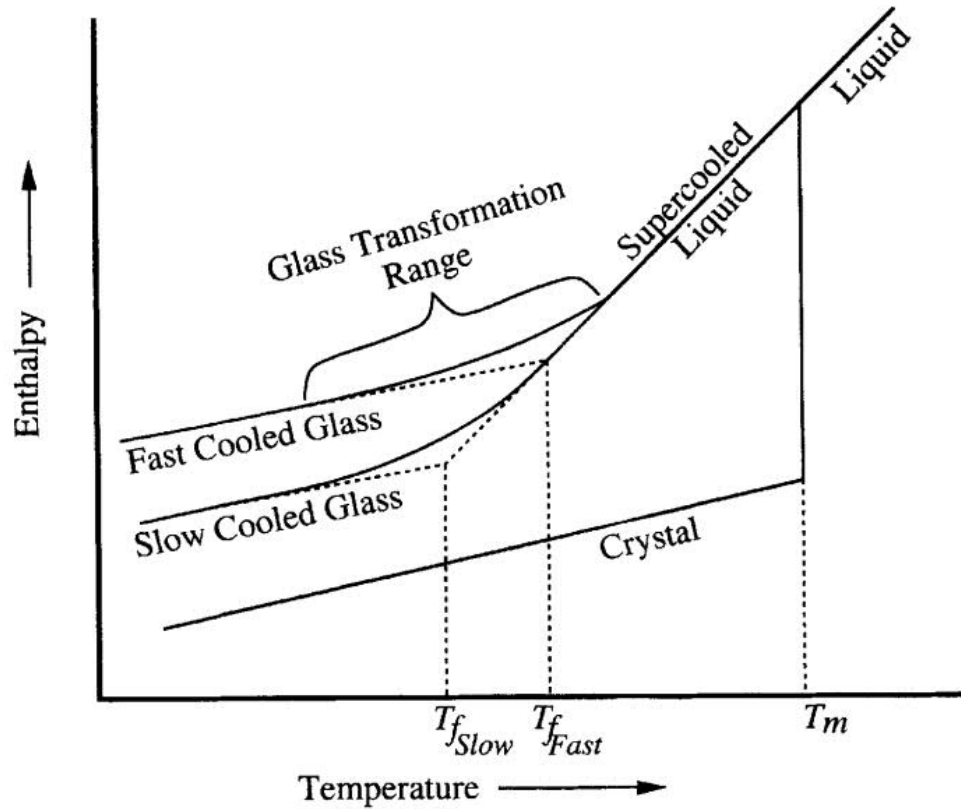
Figure 2. Schematic temperature-enthalpy curves for crystal and glass. [10, p.4]

In the curve of a crystalline material, an abrupt phase change occurs at the melting point, T_m, when the molten liquid solidifies, forming a long-range periodic structure as depicted in Figure 1a. The situation is different for the glass; the molten glass is cooled beyond the melting point without crystallizing, forming a supercooled liquid. During cooling, the internal structure of glass melt attempts to rearrange itself to minimize enthalpy. However, the exponential increase in viscosity prevents this from occurring and the melt becomes a frozen liquid. Depending on the cooling rate, the *glass transformation* from liquid to solid occurs at different temperatures, represented in Figure 2 by T_f, as the internal structure has different time to relax. [10, p.4,5]

Figure 3 shows the dependency of viscosity as a function of temperature for a typical commercial silicate glass, taken as an example.
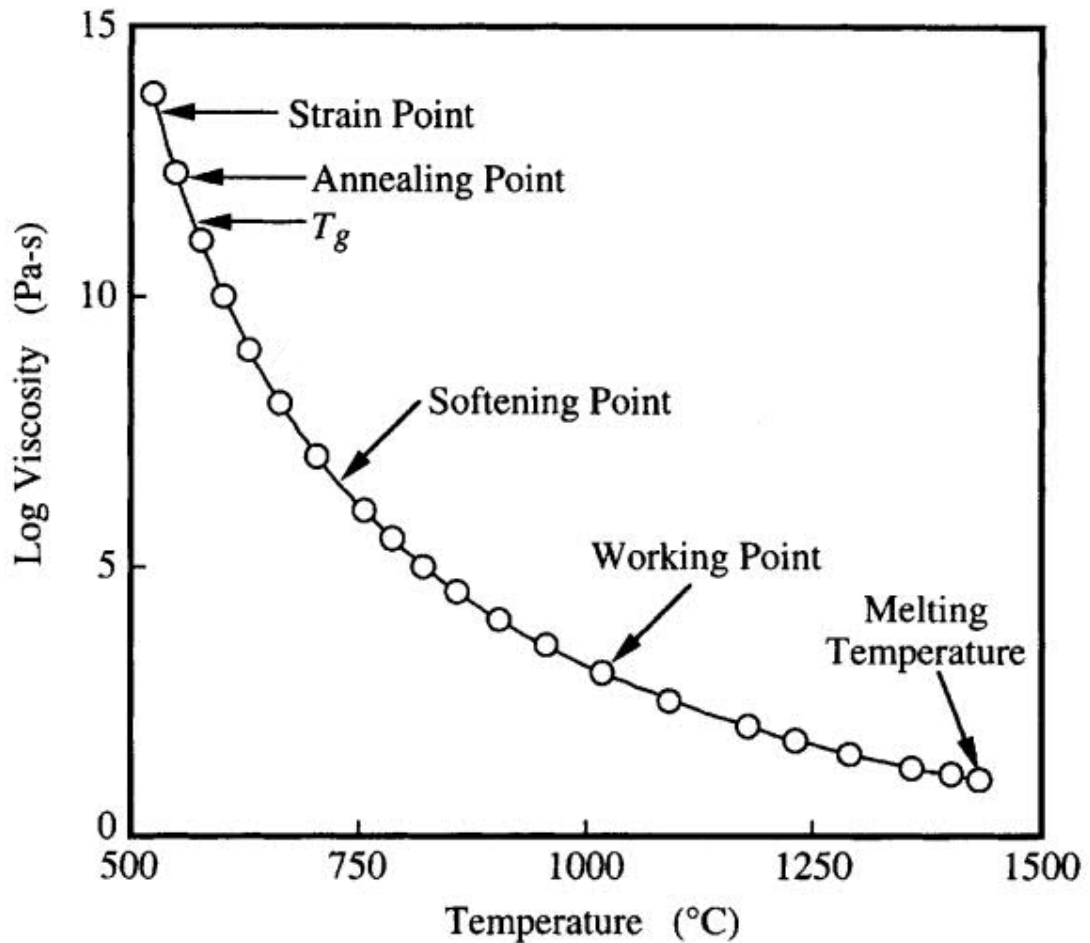
Figure 3. Schematic diagram of a silicate glass viscosity as a function of temperature. Adapted from [10, p.113].

As glass is amorphous, it has no discrete phase transition or change in viscosity. Instead, the viscosity changes gradually with the temperature.

- The *practical melting temperature* is considered as the temperature where the homogenization of the melt can occur in a reasonable amount of time and not a specific temperature corresponding to a viscosity.

- *Working point* is defined as temperature where glass viscosity is 10^3 Pa·s. At working point, the glass can be formed under stress, but will retain shape afterwards.

- The temperature and viscosity range from working point to softening point is considered as the *working range* and it is the window for traditional glass forming operations. The working range ends at the *softening point*, defined as $10^{6.6}$ Pa·s. At the softening point, the glass is viscous enough to resist deformation under its own weight.

- The *glass transformation temperature*, T_g, can be measured from heat capacity or thermal expansion measurements as a function of temperature. T_g is therefore not bound to a specific viscosity. On average, T_g corresponds to a viscosity of $10^{11.3}$ Pa·s.

- *The annealing point* is the temperature where stress is substantially relieved in few minutes. The viscosity for this point has been cited as 10^{12} or $10^{12.4}$ Pa·s, depending on source.

- *The strain point* is the point where stress is substantially relieved in few hours. It has been defined as $10^{13.5}$ Pa·s.[10, p.112,113]

Glasses are commonly fabricated using the melt quenching method that produces over 99% of all commercial glasses from windows to laser glasses. This process is the basic method of glass preparation. In melt quenching method, the raw materials are measured, heated and melted into a liquid. The molten glass is cooled sufficiently quickly to prevent crystallization and then annealed to relieve residual internal stresses from the cooling phase. Glasses can be also processed chemically from raw materials directly by the sol-gel method. In sol-gel processing, the raw materials are in a solution, which is then treated to induce gelation and so the formation of a glass network. Then the liquid is removed leading to a solid with high porosity, which can be sintered into a dense solid. Alternatively, the gelation can occur at surfaces resulting in thin films using for glass coating. [10, p.260]

2.1.2 Silica and phosphate glasses

A glass forms around a *glass former* compound, commonly silica (SiO_2), boric oxide (B_2O_3) or phosphoric oxide (P_2O_3) and forms silicate, borate and phosphate glasses respectively. These compounds form random networks by linking together with oxygen bridges. In addition to glass formers, the glass can also possess

- *intermediates* which can substitute for network formers but cannot form glasses independently e.g. Al_2O_3, TiO_2.

- *network modifiers* which disrupt network by breaking interpolyhedral linkages e.g. alkali metal oxides, alkaline earth oxides. These modifiers, also called fluxes, can be used to reduce the temperatures into more manageable levels. Different alkali metal oxides are used as fluxes with sodium and potassium oxides being the most common. Adding too much fluxing agents degrades the physical and chemical properties of the finished glass. This effect can be counteracted with property

modifiers, which improve many properties of the finished glass. Alkali earth and transition metal oxides act usually as property modifiers with calcium oxide and aluminum oxide being the most common.

Glasses can and usually contain *colorants* and *fining agents*. Colorants, as their name suggests, alter the color of the finished glass with various transition or rare earth metals. Fining agents are added into glass to aid in the bubble removal process, usually by releasing large amounts of large bubbles, which rise to the surface quickly and taking smaller bubbles with them. Alternatively, chemicals that lower the viscosity of the melt can also aid in bubble removal by helping the small and slow bubbles to rise to the top. [10, p.81-104][1, p.27-32]

Silica-based glasses are the most common basis for glasses due to the good mechanical, chemical, and optical properties of silica glass. A schematic illustration of a single linkage between two silica units is shown in Figure 4.
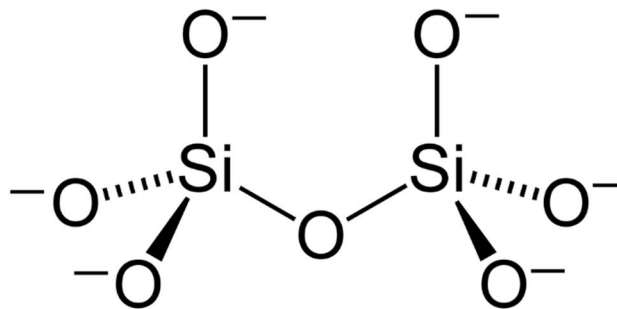
Figure 4. Two corner-linked silica tetrahedral units. [11]

Phosphate-based glasses have been for the past few decades a popular choice in photonic applications due to their better doping properties relative to silica based glasses. Phosphate glasses consist of tetrahedral phosphate units, formed from sp^3-hybridized orbitals of the outer phosphorous electrons. These electrons form covalent bonds with electrons from neighboring oxygen atoms, forming a network of P–O–P -chains, bound together with bridging oxygens. The phosphorus tetrahedra are categorized by the number of bridging oxygens per tetrahedra and denoted by Q^n -notation, where n is the number of oxygens per tetrahedra as shown in Figure 5.
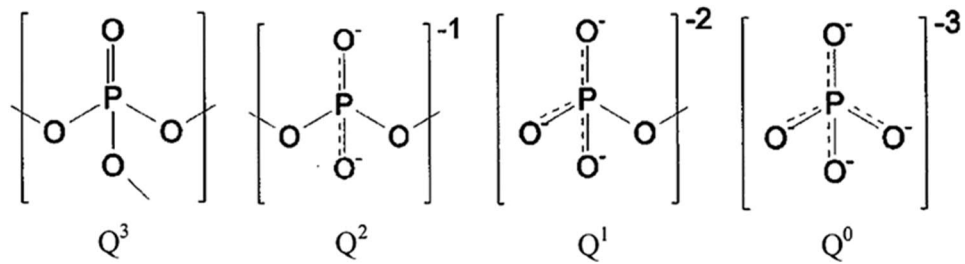
Figure 5. Schematic diagram of different phosphate units. [12]

A glass consisting solely of Q^3 phosphate units is known as *vitreous phosphate* glass, but due to its hygroscopic and volatile nature, it has received little attention in research. The addition of modifying elements breaks the bonds between tetrahedra, turning bridging oxygens into non-bridging oxygens. If a glass contains both Q^3 and Q^2 units, it is known as an *ultraphosphate* glass. Ultraphosphates are also highly reactive with moisture, limiting also their use. Replacing all Q^3 units with Q^2 units yields metaphosphate glasses. These glasses are based on linear chains of Q^2 tetrahedra. *Polyphosphate* glasses comprise of Q^2 chains, terminated by Q^1 units. Meta- and polyphosphate glasses are the most commonly studied systems due to limitations by the conventional melt processing. *Pyrophosphate* glasses consist solely of Q^1 unit dimers. As these glasses cannot form continuous random networks, they are instead based on independent tetrahedra, dimers and other fragments, linked by modifier cations. Finally, the *orthophosphate* glasses consist solely of Q^0 units.[12]

2.2 Light-matter interaction in RE elements

2.2.1 Laser glasses

The field of photonics studies encompasses the *generation, transmission, modulation, amplification, frequency conversion* and *detection* of light [13, p.vi]. Various glasses are crucial components in photonic systems. For a glass to be an effective medium for photons, it must be free from gas bubbles and other defects. Photonic glasses may however contain dopants, which amplify and convert the light [1, p.120-127].

Common dopants for light amplification and conversion are rare earth ions (RE), from the lanthanide family, which offer good spectroscopic properties due to their electron structure. A periodic table with RE elements highlighted is shown in Figure 6.

Figure 6. *Periodic table with RE elements highlighted. Adapted from [14].*

Glass provides a good environment for RE ions as it is transparent and the compositional variations allow the modification of absorption and emission bands [15], since glass can offer a wide variety of active ion sites and local fields [1, p.96,97]. Silica glass suffers from very low solubility of RE ions [1, p.111] and thus has limited dopant concentrations, a problem not present in phosphate-based glasses. Therefore, phosphate glasses offer a very attractive alternative since they offer much higher doping levels [1, p.30] together with good thermal stability and optical characteristics[12].

Trivalent RE ions have partially filled 5s and 5p electron shells providing screening effect for 4f electrons and together with Coulomb interaction and spin-orbit coupling give rise to broad variety of energy levels, leading to multiple possible states, as shown in Figure 7, and transitions for laser amplification and conversion. [1, p.90]
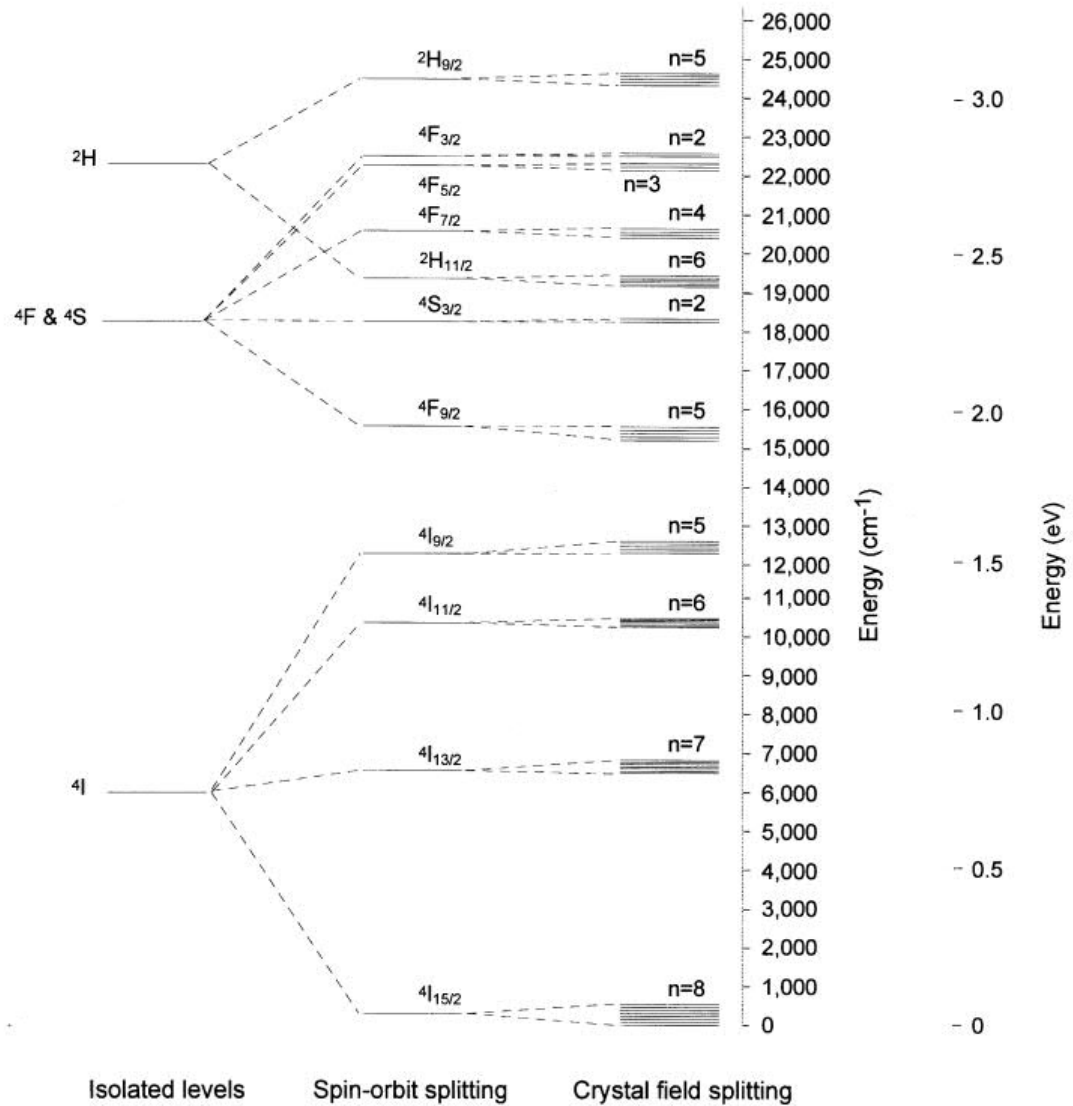
Figure 7. Various energy levels and their splitting of the Er^{3+} ion in silica.[16]

The local environment around the RE is not symmetric in glasses due to the glasses' amorphous structure. This results in splitting the energy levels even further, shown in Figure 7 as crystal field splitting. The large number energy states allows even larger amount of transitions, 56 in case of the Er^{3+} ion $^4I_{13/2}$ to $^4I_{15/2}$ -transition. At room temperature, the transitions are also subject to inhomogeneous broadening, so that the 56 individual bands broaden to form the broad emission band for Er^{3+} in glass.[16]. The crystal field splitting can be minimized in case of ordered crystalline environment, resulting in fewer possible transitions and thus higher intensity for the remaining transitions. It is therefore of interest to place the RE ions in crystals and to have these crystals in glasses.

An example of an emission band from Er:Yb co-doped glass and YAG-crystal is shown in Figure 8, centered around 1.5 μm.
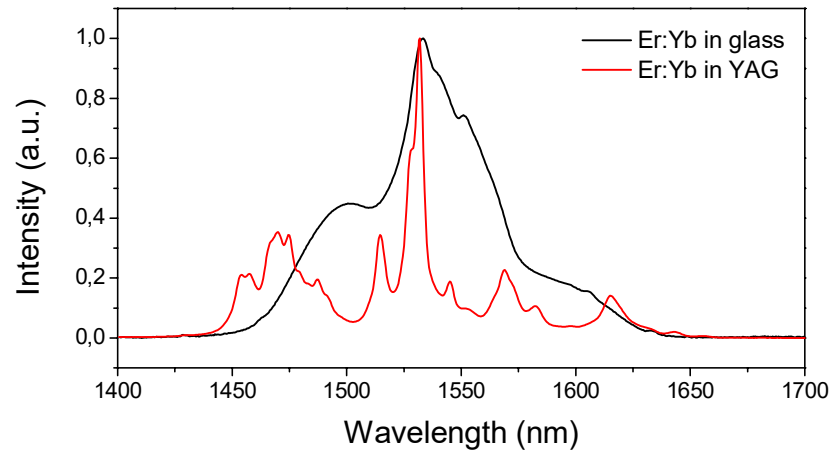
Figure 8. *Comparison of Er:Yb -doped glass and YAG-crystal emission at 1.5 µm, excited at 980nm.*

The emission band from a crystal in red presents sharp peaks, corresponding to consistent crystalline energy levels. A single broad peak, corresponding to a lack of regular structure around the RE and inhomogeneous broadening of the emission spectrum, dominates the emission band for a glass in black. [1, p.2][17]

2.2.2 Spectroscopic properties of rare-earth ions

An atom, ion, or a molecule can absorb or emit a photon during a change in its energy levels due to conservation of energy. The conservation of energy dictates that the sum of energies before the process must be the same and therefore the energy of a photon corresponds to the difference in energy levels.[13, p.434]

A schematic representation of the three processes is shown in Figure 9.
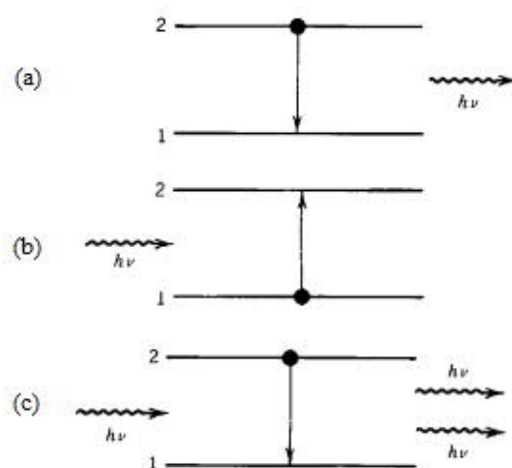
Figure 9. *Spontaneous (a), absorption (b), and stimulated emission (c). Adapted from [13]*

Spontaneous emission, shown in Figure 9a, occurs when an atom is in a higher energy level (2) and spontaneously drops to a lower energy level (1), emitting a photon (hv) in the process. The process is spontaneous because it is independent of the number of photons present. The emission wavelength is determined by the difference in energy levels of an atom, which is in turn determined by the atoms electronic structure. The local environment around the atom therefore determines the optical response.

Absorption, in Figure 9b, occurs when an atom is in the lower energy level and the incoming photon has sufficient energy to raise the atom to a higher energy level.

Stimulated emission in Figure 9c, occurs when an atom is already in an higher energy level and an incoming photon's energy closely matches the difference in energy levels. Here, the incoming photon may stimulate the emission in the atom, where the atom emits an identical photon while relaxing to the lower level. This process effectively clones the incoming photon and is the basis for laser amplification.

The absorption and stimulated emission are dependent on the number of photons present with the probability increasing with increasing number of photons [13, p.435,436]. The two level system is the simplest system, but actual systems have many energy levels with complex transitions. These complex systems can be explained by using simplified three- and four-level systems, shown in Figure 10. [86,87]
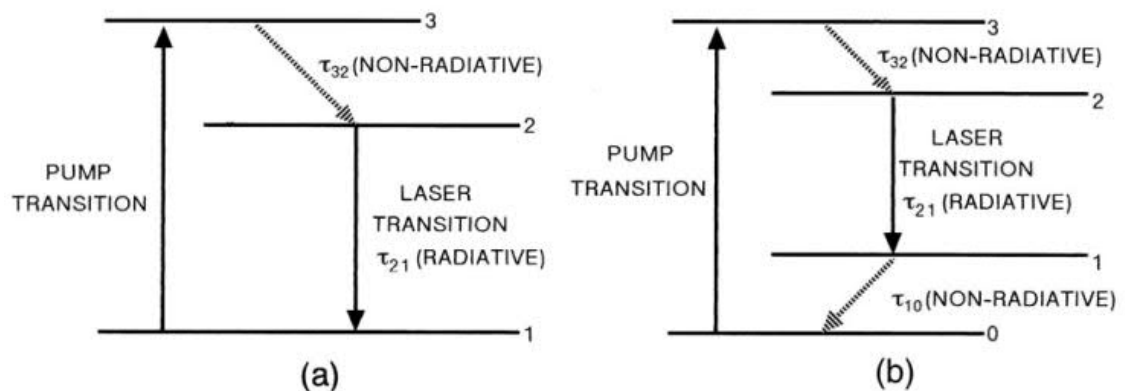
Figure 10. Three-level (a) and four-level (b) energy diagram. Adapted from [1, p.87]

In a three-level process (Figure 10a), an atom first absorbs light, rising from energy level 1 to 3. This process is more commonly known as optical pumping. From level 3, the atom decays rapidly to level 2 in a non-radiative transition, dissipating the excess energy as heat. From level 2, the atom decays via stimulated emission back to its ground state, amplifying light in laser action. The four-level system improves on the three-level one by introducing an additional non-radiative transition after the stimulated emission (Figure

10b). This system ensures that excited atoms are present even at low pumping pow-ers.[1, p.86,87]

A system may contain more than one dopant and this opens up new possibilities as excitations may transfer between dopants. This way, pump absorption and lasing are decoupled and independently optimized. Figure 11 shows the energy level system for erbium (Er^{3+}) and ytterbium (Yb^{3+}) codoping. [18]
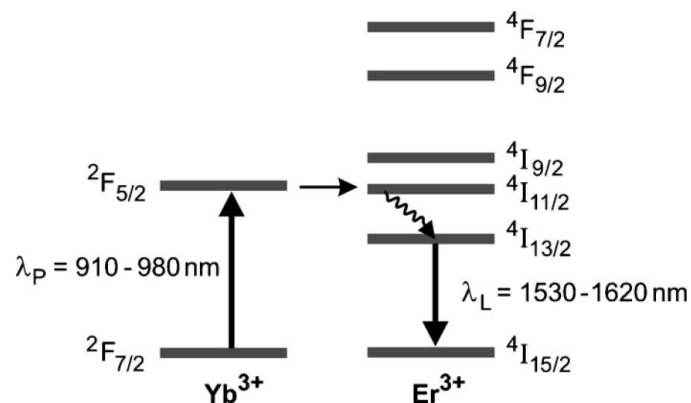
Figure 11. Energy level diagram for Er:Yb co-doping. [18]

This system acts essentially as a three-level system with Yb^{3+} absorbing the pump light, transferring the energy to Er^{3+}, where it experiences a non-radiative transition, followed by a stimulated emission. This setup reduces pump wavelength demands and increases energy transfer efficiency, allowing higher powers. [18].

Atoms may also co-operate by transferring energy from one atom to another one, as depicted in Figure 12 where A and B represent two atoms, both excited to higher level when one (A) gives its energy to other (B).
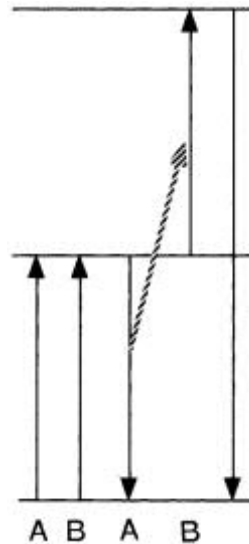
Figure 12. *Co-operative up-conversion. Adapted from [1, p.94]*

In this process, A returns to the ground state and B is excited to even higher level, from where it may relax to the ground state and emit a photon with energy equal to the sum of the two photons required to excite A and B in the first place. This process is known as *up-conversion*. [1, p.96]

2.2.3 Raman scattering

All atoms have some thermal movement and therefore have different low-energy states with different vibrational energies, known as phonon states. These energies, shown in Figure 13 as $\hbar\Omega$, are very small compared to energies found in electronic transitions, but they exist. Therefore, these states also take part in transitions, but they are difficult to detect as individual transitions. [19, p.22,23]
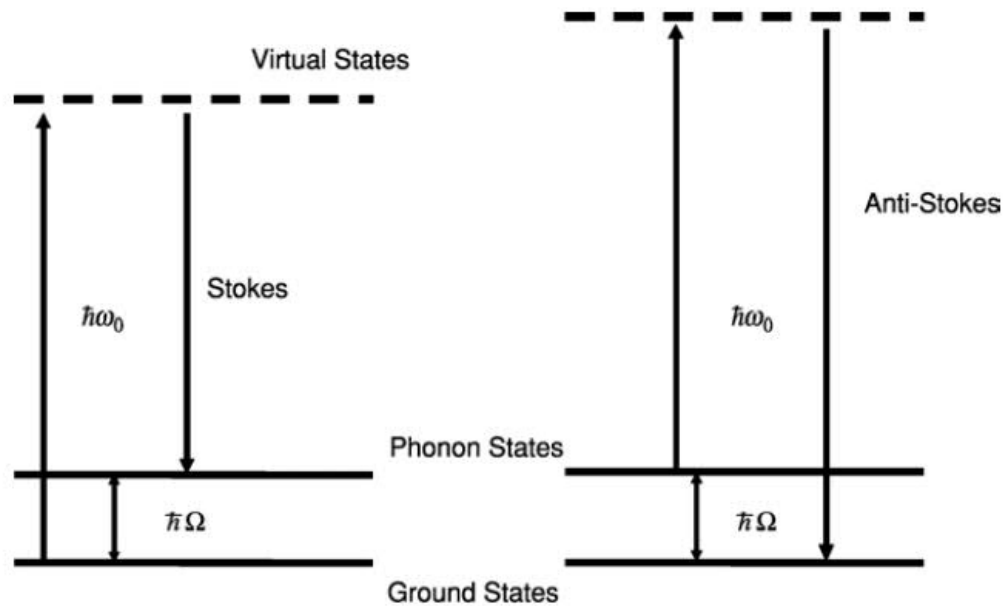
Figure 13. Energy level diagrams for Stokes and anti-Stokes shifts in Raman scattering. [19, p.32]

We can think that an atom absorbs a photon ($\hbar\omega_0$) and is excited to a virtual energy state. Immediately after this, the atom relaxes back to a state with higher vibrational energy and therefore the emitted photon is shifted to slightly longer wavelength. This process is known as Stokes shift. This process can occur also in reverse, i.e. photon absorption from vibrational state to the virtual state and back to ground state. This process is known as anti-Stokes shift and results in photons with slightly shorter wavelengths. In reality, no absorption or emission occurs, rather it is inelastic scattering between the atom and photon, known as Raman scattering. The virtual states are a useful concept in understanding this process. The Raman spectra provides information on available vibrational energies in the sample and thus information on the structure. [19, p.28-32]

2.3 Glass-ceramics

2.3.1 Definition of glass-ceramic

A glass-ceramic (GC) is a glass that contains crystals. These crystals can precipitate in the glass after heat treatment. By controlling the temperature and time of the heat treatment, controlled growth of nano- and/or microcrystals can occur. [10, p.256,257] The spectroscopic properties of Er^{3+} ions can be enhanced if these crystals contain RE [1, p.132]. Compared to glasses, glass-ceramics exhibit higher absorption and emission cross-sections and longer lifetimes. The glass-ceramics need to be also transparent to avoid light scattering. In scattering, an incident ray of light deviates from its original path

without transferring energy between the particle and light. [20, p.67] Therefore, it is crucial to control the crystals size and composition in the glass and crystals for the fabrication of transparent glass-ceramics.

The theory regarding the scattering of electromagnetic waves from spherical particles is known as Mie theory, named after its publisher. The Mie theory encompasses multiple complex mathematical equations, which are out of the scope of this work. The Mie theory gives solutions to Maxwell's equations for electromagnetism when a plane wave is scattered from a homogenous sphere. Mie theory is most useful in describing scattering when the particle size is on the order of wavelength.[21] Using the Mie theory, transmittance of light at 808 nm at different crystal sizes and differences in refractive index can be calculated [5] and results are shown in Figure 14.
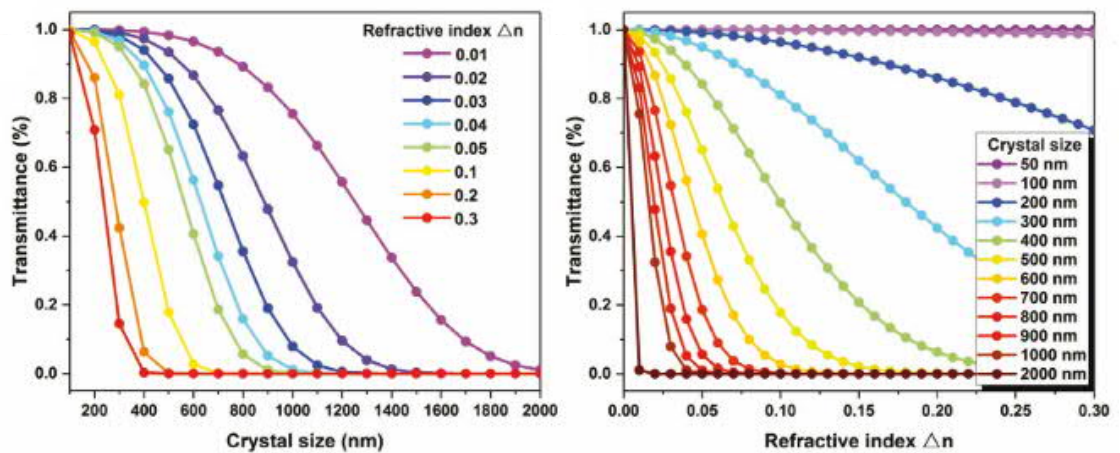
Figure 14. Effect of crystal size and change in refractive index on transmittance at 808nm based on Mie theory. Adapted from [5]

In order to obtain transparent glass-ceramics, the particle size must be small, preferably smaller than the wavelength and the refractive index mismatch between the glass and particle as small as possible.

The first glass-ceramics in photonics [22] in were not transparent due to large size of crystallites. Since then glass-ceramics with crystallites smaller than wavelength of visible light have been realized [23] and thus transparent glass-ceramics have been made.

2.3.2 Crystal nucleation and growth in glass

As we know, glass structure differs from that of crystalline material. Glass can be transformed back into crystalline state by appropriate thermal treatment. During crystallization, the glass is transformed from its unorganized phase with high free energy, to an organized phase with lower free energy. Crystallization begins with nucleation, in which the amorphous material rearranges its structure, forming nuclei. Nucleation can occur by

itself, without external surfaces, in *homogeneous nucleation,* or around some external surfaces such as dirt or impurities in *heterogeneous nucleation.* [24]

The classical nucleation theory describes the homogeneous nucleation process, in which small nuclei are formed throughout the glass. For a spherical particle, transition to into crystalline phase reduces the bulk volume energy as the particle radius increases and more and more of the material is now in the lower energy state. At the same time, formation of an interface between the nucleus and the melt requires energy, leading to an increase in interfacial energy. These energies as a function of a hypothetical particle radius are shown in Figure 15, together with the sum of these two energies, total energy in green.
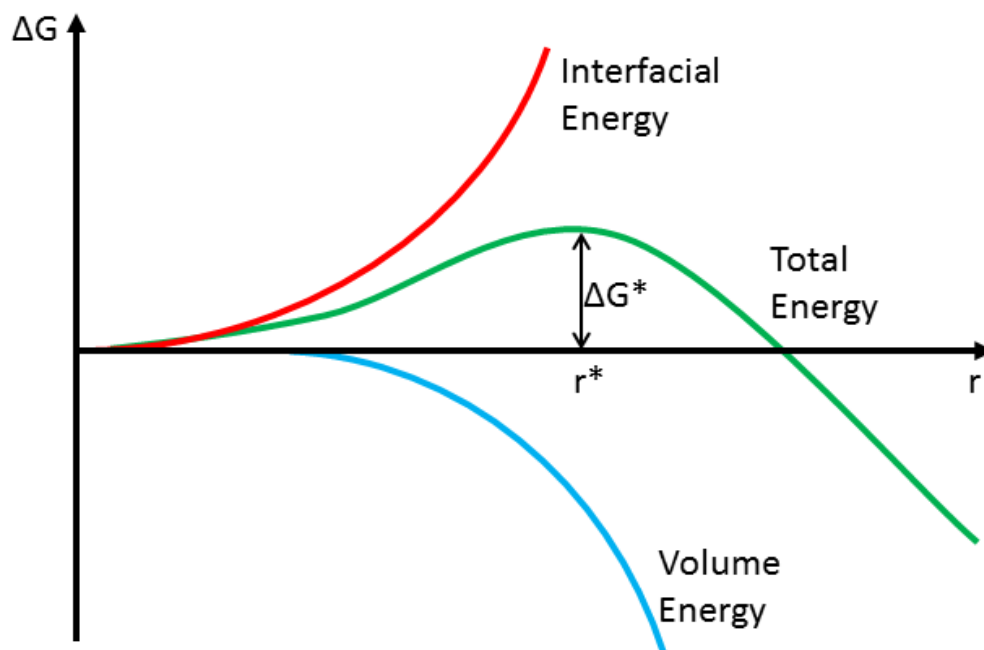
Figure 15. *Schematic diagram of bulk free energy, ΔG, as a function of particle radius. Redrawn from [24].*

Figure 15 shows that the interfacial energy contribution dominates at small particle sizes and only at larger particle radii, the nuclei become stable as the volume energy begins to dominate. Therefore, a barrier to nucleation exists at the critical radius, r^*, corresponding to a barrier energy, ΔG^*. Overcoming this barrier requires careful control of the temperature, as can be seen from the nucleation curve in Figure 16.

The key to manufacturing transparent GCs is in controlling the nucleation and growth of the crystallites.[25] Processing of glass ceramics starts from a base glass, usually prepared by melt quenching. This glass is then heated for a certain period at a nucleation

temperature to form the crystal nuclei and the temperature is increased to grow the crys-
tallites to the desired size.[25] These two stages are called nucleation and crystal growth.
Figure 16 shows schematically how crystal nucleation and growth are dependent on the
temperature.
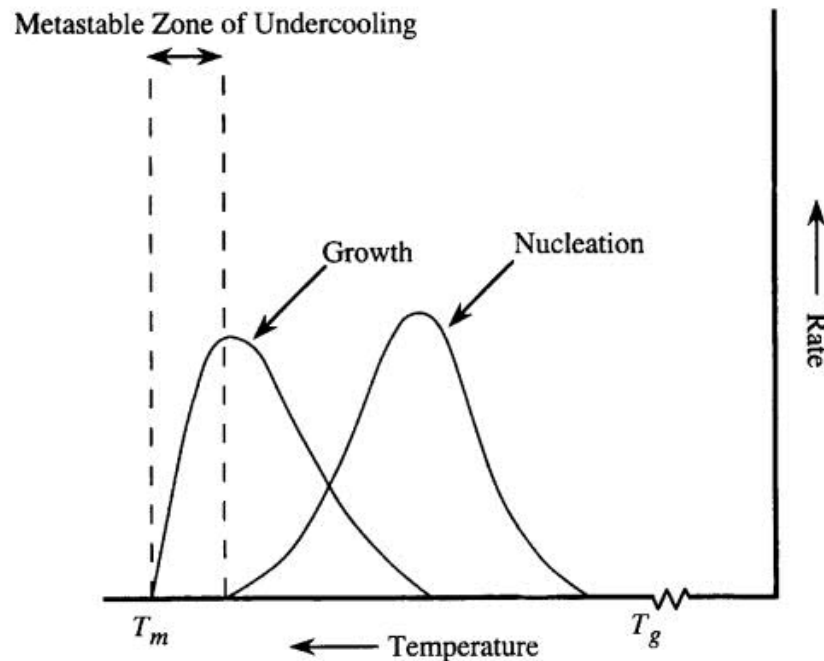
Figure 16. Temperature dependence on crystal nucleation and growth rates.[10]

If the nucleation rate is high and growth rate is low, large number of nanoscale crystal
nuclei will form, but the crystals will not grow very much, resulting in a large number of
tiny crystallites. Inversely, at high growth rates and low nucleation rates, the initial num-
ber of nuclei is low but the ones that do form, grow into large crystals. For transparent
glass ceramics, the crystallite size should be minimal as larger objects scatter light more
effectively.[25] The crystals should also precipitate inside the glass, not at the surface.

2.3.3 Crystal containing glasses

The controlled nucleation and growth process has some limitations: the most important
one being that not all glasses undergo bulk precipitation of rare-earth doped crystals.
Another technique to fabricate a glass, which contain rare-earth doped crystals homoge-
neously distributed in the volume, is to embed RE doped particles directly into the glass
as illustrated in Figure 17.
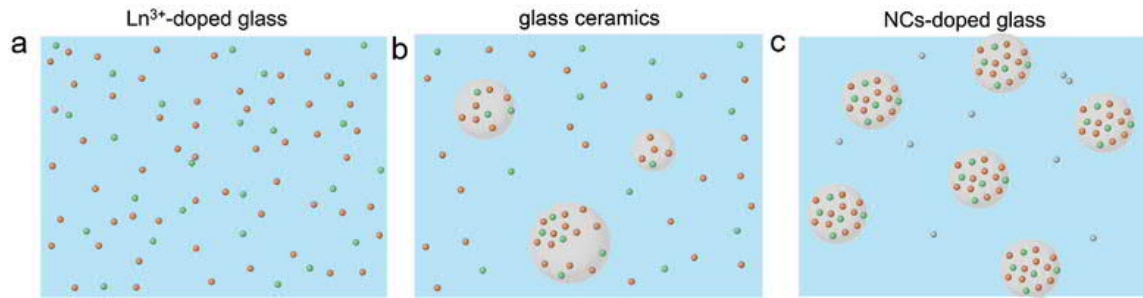
Figure 17. *Schematic diagram of different RE doping methods: RE-ion doped glass (a), glass ceramics (b), and particle-doped glass (c). Adapted from [6].*

Preparing the particles separately from the glass provides more options over *in situ* preparation, as more synthetization techniques and methods are available. Preparing the particles separately from the glass gives control over their size, shape, composition and nanostructure independently of the glass composition.[6] These particles can be added in the glass melt as illustrated in Figure 18.
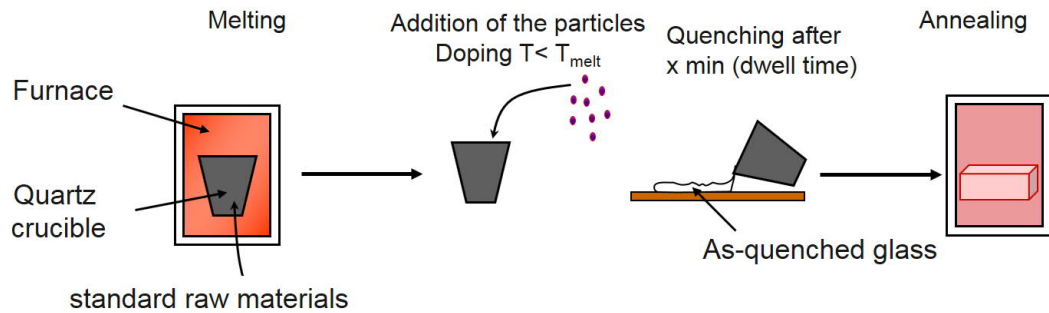
Figure 18. *Schematic diagram of the direct doping method.*

In the direct doping, the glass is prepared normally, i.e. as in the melt-quenching method, but before quenching, particles are added directly to the melt. The glass is allowed to dwell in order to disperse the particles and finally the glass is quenched and annealed.

Adding the particles to the raw materials or re-melting powdered glass with embedded particles might sound attractive, but in reality, it can lead to particle dissolution and degradation due to corrosive and hot environment as explained in [3]. To avoid degradation and dissolution of the particles, the particles must be added directly into molten glass. By controlling the temperature and time; the survival of the particles can be achieved [6], but at the cost of homogeneity since the particles may not disperse sufficiently rapidly.[3]

2.3.4 Sintering

The other option for the preparation of particle containing glasses is to prepare a mixture of powdered glass and particles and then sinter the mixture into a solid. [8, 26] Sintering

is a process, which allows forming solid bodies from powders without melting. Sintering uses heat and/or pressure to join particles together, densify and eventually form a solid piece.[27] Glass sintering at temperatures below the melting point is dominated by viscous flow mechanism [27], theory of which was developed by Frenkel[28].
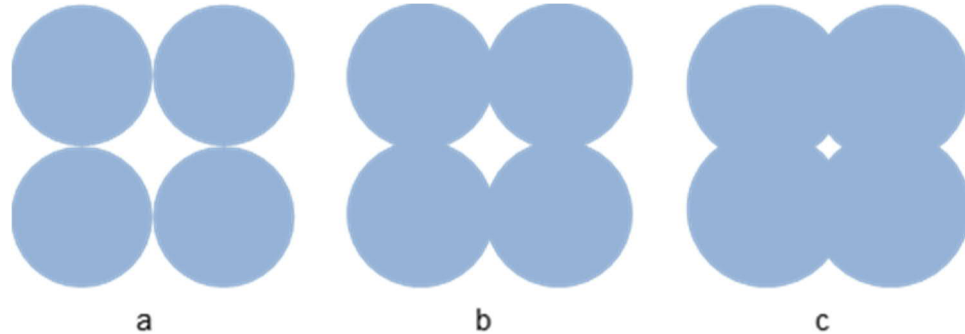
Figure 19. *Sintering progress from separate particles (a) through necking stage (b) to mostly dense solid (c).*

Sintering begins when particles come in contact (Figure 19a) and material begins to flow to form a neck between the particles (Figure 19b) as this minimizes the surface energy caused by surface tension. [27] The material transport continues and tiny pores or bubbles form in the otherwise solid material (Figure 19c). The glass is highly viscous. Further densification is necessary for transparent glass, but this requires additional pressure.[26]

The shrinkage of uniform spherical particles with radius R is given

$$\frac{\Delta V}{V_0} = \frac{9\gamma}{4\eta R} t,$$
(1)

where $\frac{\Delta V}{V_0}$ is volumetric shrinkage relative to original volume, γ is surface tension, η is viscosity and t is time.

From equation 1, the rate of shrinkage, i.e. rate of densification, is proportional to the surface tension and time and inversely proportional to viscosity and particle radius. Surface tension is largely dependent on the material properties and temperature. However, for our sintering temperature regime, the surface tension is considered to be constant.[29] Viscosity of glass is inversely proportional to temperature [10, p.247] and therefore higher temperatures are preferred in sintering. The maximum available temperature is however, limited by the glass crystallization temperature. From equation 2, we find that

$$\frac{\Delta V}{V_0} \propto \frac{Tt}{R},$$
(2)

where T is the sintering temperature and R is the particle radius.

Thus the sintering requires high temperatures, which are limited by crystallization, small particle size, which is limited by milling and pulverizing equipment, and time, which has some practical limitations.

According to former research [8, 26], the fabrication of clear glass from powdered glass does not work by using only temperature and time. This is due to the pores left in the glass, which scatter the light and render the glass opaque. These pores or bubbles cannot be removed in a reasonable amount of time at temperatures below crystallization. However, an increase in pressure improves the sintering performance and allows closing these pores leading to the fabrication of optically transparent glass. [8, 26]

The pressure difference between the outside and inside, ΔP, surface tension, and radius of curvature, r, correlates according to [10, p.44].

$$\Delta P = \frac{2\gamma}{r}. \tag{3}$$

Therefore, any additional external pressure will add on to the internal pressure, which will increase the pressure inside the bubble reducing its radius and so the scattering as the bubbles are smaller. [10, p.44]

3. EXPERIMENTAL

3.1   Preparation of the glasses

3.1.1 Glass systems

This work was based on incorporating various particles into a host glass with various methods. The particles to be added were $Eu^{2+,}Dy^{3+}$ -doped $SrAl_2O_4$ microparticles, erbium, ytterbium co-doped yttrium aluminum garnet (YAG) nanoparticles, erbium and ytterbium co-doped sodium yttrium fluoride ($NaYF_4$) nanoparticles, and erbium doped glass ceramic (GC) microparticles. The host glass composition in mol-% was 90 $NaPO_3$ - 10 NaF and was selected for its low melting point and existing previous research regarding particle containing glasses.[2]

Different techniques to prepare the particles containing glasses were used

1) The particles were added in the glass batch prior to the melting and the mixture was melted using standard melting process

2) The particles were added in the glass melt using the direct doping method

3) The particles were mixed in the glass crushed into powder and the mixture was hot pressed.

Various concentrations of particles were tried in order to optimize the dispersion, quantity and survival of the particles. Table 1 summarizes the investigated glasses.

Table 1.   *Particle containing glasses by method, particle and mass concentration.*

	In batch	In melt	Sintering
YAG	5 wt.%	2.5 wt.%	5 wt.%
GC	10 wt.%, 50 wt.%	5 wt.%, 9 wt.%	5 wt.%
NaYF$_4$	-	-	5 wt.%

In melt and in batch -samples had a batch size of 6 grams, except for the 5 wt.% and 9 wt.% GC in melt samples were prepared as 10 gram batches, in an attempt to improve particle dispersion in the doping stage. The sintering was done on 1 gram samples.

3.1.2 Synthesis of the particles

The YAG particles were prepared at the Institute for Solid State Chemistry Bordeaux, ICMBC (France), prior to this study. The particles were synthesized by self-combustion process and a following thermal treatment. Aqueous yttrium, ytterbium, erbium and aluminum nitrates were mixed with glycine fuels. The mixture was heated to 250 °C, leading in auto ignition and combustion and resulting in the formation of brown powder. This powder was then heated from room temperature to 1000 °C at 15 °C/min and held at 1000 °C for 4 hours and then allowed to cool back to room temperature naturally. The resulting powder was then ground in a planetary mill into finer particles, which were then dispersed in water. A core-shell structure with 5 nm layer of SiO_2 was then formed around the YAG particles. YAG particles from previous step were cleaned with nitric acid to remove leftover compounds and surface defects. The particles were then stabilized with citrates to prevent agglomeration. Citrated YAG is added into a tetraethyl orthosilicate (TEOS) solution to produce the SiO_2 shell via the sol-gel condensation reaction. Finally, the particles were washed, dried and calcined at 800 °C for 3 hours in order to remove residual chemicals.

Erbium, Ytterbium co-doped sodium yttrium fluoride ($NaYF_4$) nanoparticles were prepared at University of Turku (Finland) prior to this study with a process described in [30]. To prepare these particles, NaF (2.1 g) was dissolved in distilled water (60 ml), to which was added 0.2M yttrium(III) chloride (18 ml), ytterbium(III) chloride (3.4 ml) and erbium(III) chloride (0.6ml). A Na/Er ratio of 12.5 was used to ensure the formation on $NaErF_4$ phase instead of $NaErF_3$. The solution was stirred for 1 hour and the precipitate was then separated with centrifuge. The precipitate was washed three times with water and once with ethanol. After each washing, the precipitate was separated with a centrifuge. The precipitate was then dried in a vacuum desiccator. Annealing was done at 500 °C for 5 hours in 90 N_2 - 10 H_2 atmosphere to change the crystal structure to hexagonal structure. This was followed by natural cooling back to room temperature in the same atmosphere. [30] Before being processed by sintering, the powder was ground into a fine powder with a mortar and a pestle.

The glass-ceramic (GC) powder was prepared from standard raw materials. The glass-ceramic had a composition of 99 (75 $NaPO_3$ - 25 CaF_2) - 1 Er_2O_3 (in mol%). This composition was chosen, because it has been shown that the glass-ceramic has enhanced upconversion properties compared to the parent glass [31]. The glass was first prepared

from sodium hexametaphosphate, calcium fluoride (CaF_2) (Alfa Aesar, *99.95%*) and er-bium(III) oxide using the melt quenching method. The glass was melted in a quartz cru-cible at 950 °C for 5 minutes before quenching on a brass plate and annealing at 200 °C for 6 hours. Afterwards, the glass was subjected to thermal treatment to induce crystal nucleation and growth. The glass was held at 20 °C above its glass transition tempera-ture, 300 °C, for 17 hours to create crystal nuclei and then at the first peak crystallization temperature, 375 °C, for 6 hours to grow the crystals fully into glass-ceramic. The GC was crushed into fine powder with a mortar and a pestle. Unsieved and sieved (sub-38µm) powders were used in this study with unsieved used in direct doping and sieved in sintering process.

Commercial $Eu^{2+,}Dy^{3+}$ -doped $SrAl_2O_4$ microparticles (Jinan G.L. New Materials, China, BG-01) were used. These particles have long luminescence lifetime in the order of minutes, which allows visual observation of particle distribution and also possible par-ticle degradation from changes in emission spectra and lifetime. These particles have been used previously [3, 7, 32] to observe changes during direct doping process and therefore possible changes to particle composition or structure are known. It has been found that the decomposition of the particles can be associated with Eu^{2+} oxidizing from to Eu^{3+} and with the reduction in the luminescence intensity [7].

3.1.3 Standard melting process

Glass making in general starts from a batch calculation. Batch calculation begins with a stoichiometric equation describing the starting materials on one side and finished prod-ucts on the other side. The average molar mass of the finished glass is first calculated as a weighted average of the elements and their respective fraction in the finished glass according to

$$M_{glass} = \sum x_i M_i, \tag{4}$$

where   is the molar mass of the finished glass, x_i is the molar fraction of an element to be calculated and M_i is the molar mass of the element or compound to be calculated. The mass of the finished glass to be manufactured is divided by the molar mass from Equation 4 to give us the average molar amount of glass according to

$$n_{glass} = \frac{m_{glass}}{M_{glass}}, \tag{5}$$

where m_{glass} is the mass of finished glass to be made and n_{glass} is the amount of glass in moles.

From the molar amount of finished glass, individual components of the finished glass are calculated according to

$$n_i = x_i n_{glass},\tag{6}$$

where n_i is the molar amount of an individual component in the finished glass.

From the stoichiometric equation describing the glass formation reaction, the amount of each precursor is deduced. From there, the masses of each individual precursor is finally calculated according to

$$m_i = n_i M_i,\tag{7}$$

where m_i is the required mass of an individual precursor.

The host glass had a composition 90 $NaPO_3$ - 10 NaF, in molar percentages. The glass was prepared using sodium hexametaphosphate $(NaPO_3)_6$ (Alfa Aesar, *tech.*) and sodium fluoride (NaF) (Sigma-Aldrich, *99.99%*). The precursor chemicals were weighed, mixed and crushed by hand with a mortar and a pestle. The particles were mixed with the glass batch. The mixture was melted in a quartz crucible at 750 °C for 5 minutes before quenching in a brass mold and annealing at 200 °C for 6 hours. More information about this glass can be found in [4].

A reference glasses were also prepared. These glasses contained erbium(III) oxide (Er_2O_3) (Sigma-Aldrich, *99.9%*) and ytterbium(III) oxide (Yb_2O_3) (Sigma-Aldrich, *99.9%*) with compositions of 99 (90 $NaPO_3$ - 10 NaF) - 1 Er_2O_3 and 99 (90 $NaPO_3$ - 10 NaF) - 0.5 Er_2O_3 - 0.5 Yb_2O_3 (in mol%). These glasses acted as a reference case and enabled us to study the RE site and distribution in glass and particles.

3.1.4 Direct doping method

A second series of glass was prepared by the direct doping method. The host glass was melted at 750 °C for 5 minutes, held at 550 °C for 20 minutes to stabilize temperature and then the particles were added into the molten glass and held at 550 °C for 3 minutes to disperse the particles prior to quenching the glass. Afterwards, the glasses were annealed at 200 °C for 6 hours. Details of this technique was reported in [2, 4].

3.1.5 Hot pressing method

For sintering, the glass host was melted as described previously. After annealing the glass was crushed into powder. The powder was sieved to different particle size ranges,

with sub-38μm being used for sintering. Powdered glass was sintered using hydraulic press combined with a tube furnace (Mti Corp., USA, YLJ-HP6), shown in Figure 20. A graphite die with alumina rods were used in our setup, as they were required to reach the necessary temperatures.
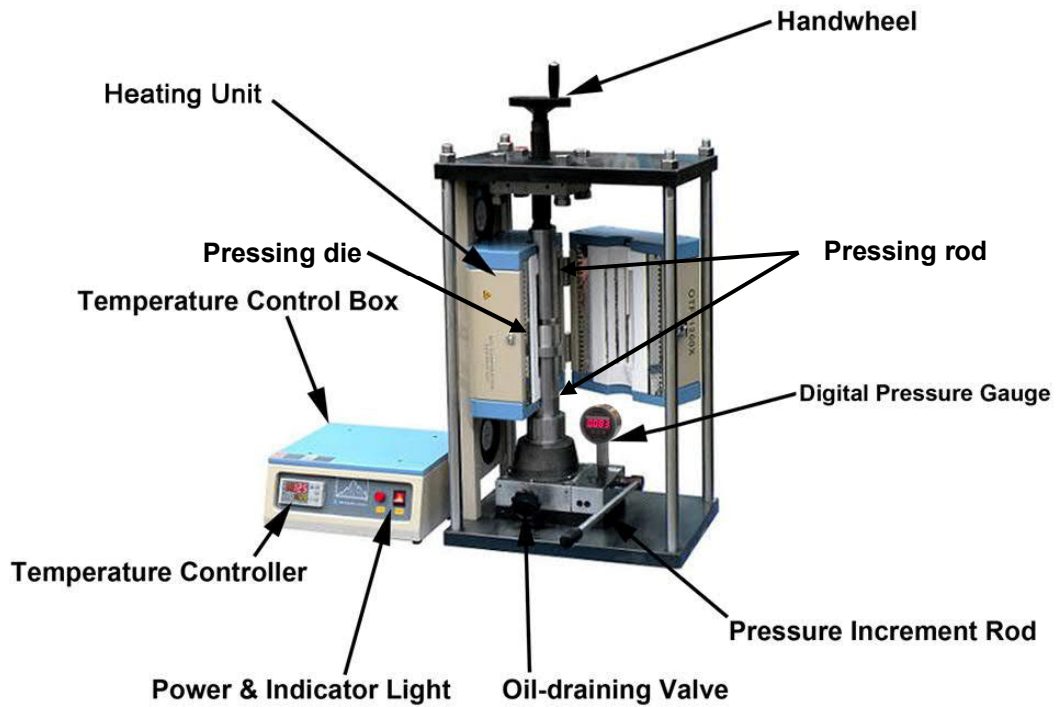
Figure 20. Hot uniaxial press setup, shown with steel rods and die. Adapted from [33].

The process of preparing transparent glass begins in measuring glass powder and any desired dopants. The powders are mixed very thoroughly to ensure as homogenous particle distribution if the glass has dopant particles. Meanwhile, the graphite pressing die, in Figure 21, is cleaned with ethanol to minimize carbon contamination. The glass powder is then placed in the mold, between 2 graphite tools.
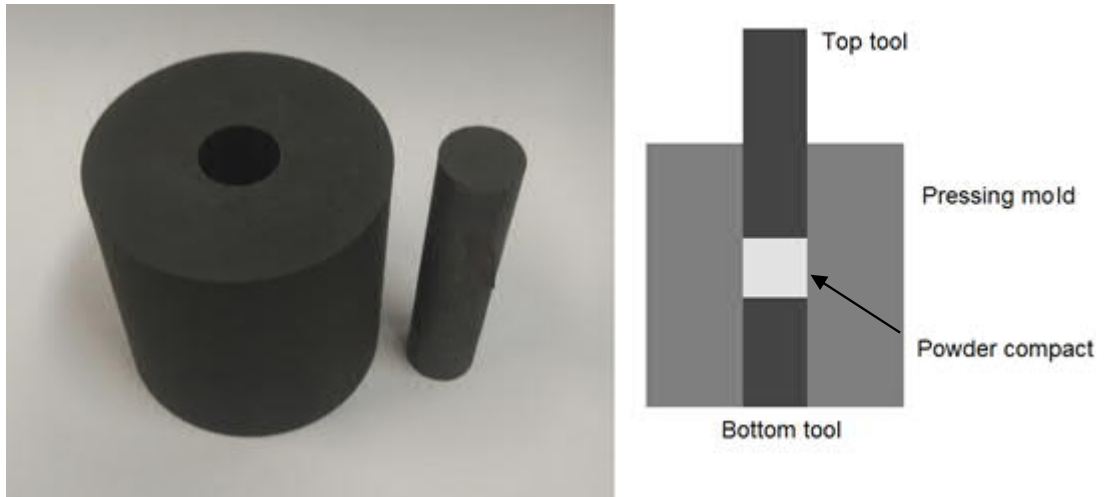
Figure 21. Picture and a schematic diagram of the graphite die.

The ready pressing die assembly can now be placed in the furnace, between 2 alumina pressing rods. The die and the rod is centered to ensure even heating. The die is then secured by tightening the hand wheel at the top and closing the furnace. The heating program is programmed into the temperature controller and heating is started (step 1 in Figure 22).
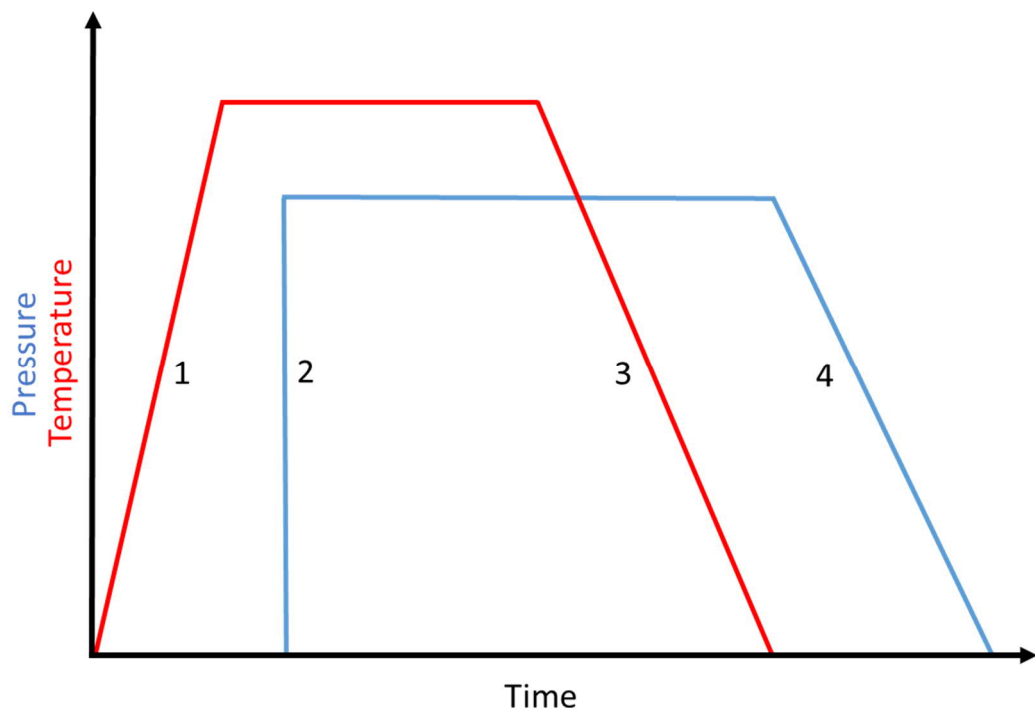
Figure 22. Schematic diagram of the sintering cycle.

When it is time to increase pressure in the die, the oil-draining valve is closed tightly and the pressure increment rod is pumped to desired pressure (step 2 in Figure 22). At the beginning, the pressure will drop as the powder compacts and densifies, but after about

1 hour most of the compaction has occurred. The pressure was controlled and increased occasionally to counteract minor pressure leakage in the system and also during cooling periods, as the pressure drops due to thermal contraction (step 3 in Figure 22). Pressure is then released slowly to prevent the glass from shattering (step 4 in Figure 22). The finished glass is then removed and the die cleaned for the next use.

3.2   Thermal analysis

The thermal properties of the glasses were determined using differential scanning calorimetry (DSC) on Netzsch Jupiter F1. In DSC, the change in heat flow is measured as a function of temperature. A sample and a reference crucible are heated at a constant rate while the DSC measures the required energy to do so.[34] As phase changes require additional energy, the DSC records an endothermic drop in heat flux, signaling a glass transition for example. Alternatively, the crystallization releases significant amounts of energy and this release of energy results in an exothermic peak on the *thermogram,* graph presented in Figure 23.
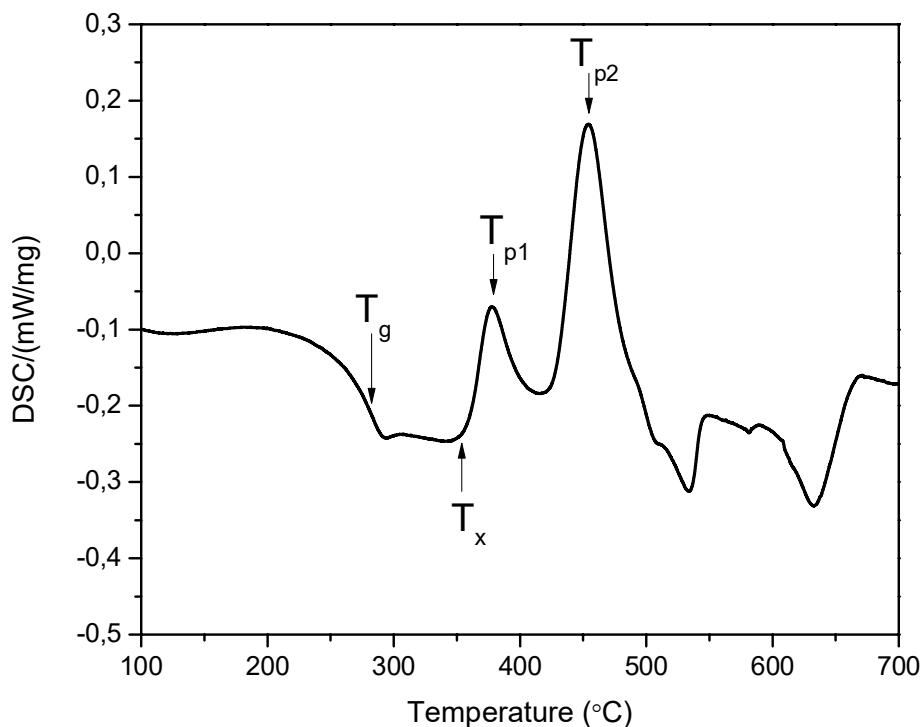
Figure 23. Thermogram of a glass ceramic sample taken as an example

Powdered glass samples of approximately 30 mg were heated at 10 °C/min in platinum crucibles and N_2 atmosphere. The glass transition temperature is taken as the inflection

point, marked as T_g. Onset of crystallization is marked by T_x, indicating the beginning of crystallization. The crystallization peak was the maximum exothermic peak, T_p. In Figure 23, two different peaks can be seen, corresponding to different crystalline phases [10, p.239]. Accuracy of these measurements was ±3 °C.

3.3   Density measurement

The densities of glasses were measured using Archimedes' method in ethanol. Measurements were performed on OHAUS Adventurer Analytical -scale, equipped with a density measurement kit. Density measurement works by weighing the glass in air and the while immersed in liquid, here ethanol. Then, the density of the glass can be calculated form

$$\rho_{glass} = \frac{m_{air}}{m_{air} - m_{EtOH}} \rho_{EtOH},$$ (8)

where ρ is the densities of glass and ethanol, m is the mass in glass in air and ethanol, indicated by subscripts. Accuracy of these measurements was ±0.02 g/cm³.

3.4   Light absorption measurement

The absorption spectra were measured using a double beam spectrophotometer Perkin Elmer LAMBDA 1050. A schematic diagram of it is shown in Figure 24.
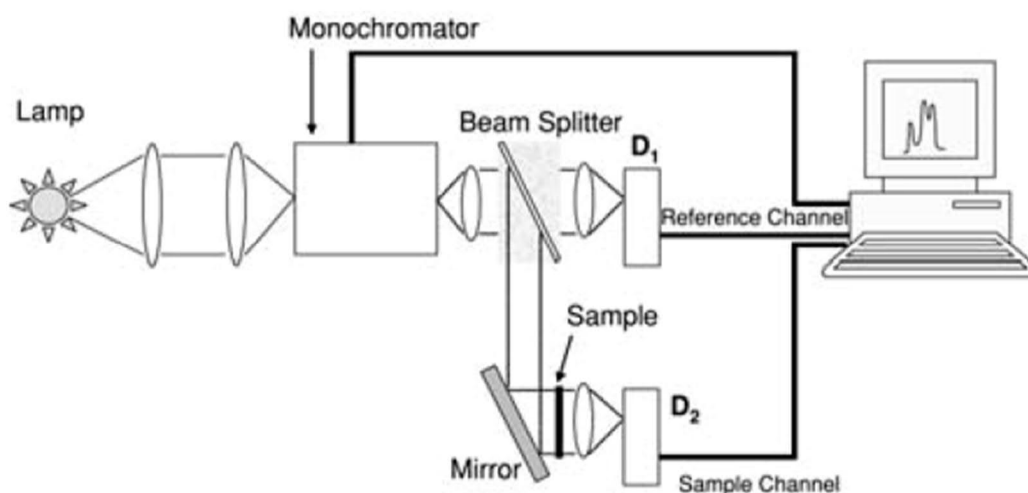
Figure 24. Schematic diagram of a double beam spectrophotometer. [19, p.12]

A broadband light source is passed through a monochromator, which selects a specific wavelength to pass. The light beam is then split into two, one passes through the sample before reaching detector and the other goes directly to a detector. The detector signal is

compared at different wavelengths and the transmittance of the sample is recorded. Transmission was recorded from 300 nm to 1700 nm at 1 nm intervals and a 2 nm slit.

3.5 Light emission measurement

The emission spectra were measured using a spectrofluorometer laboratory setup built at Tampere University. A schematic diagram of the device is shown in Figure 25.
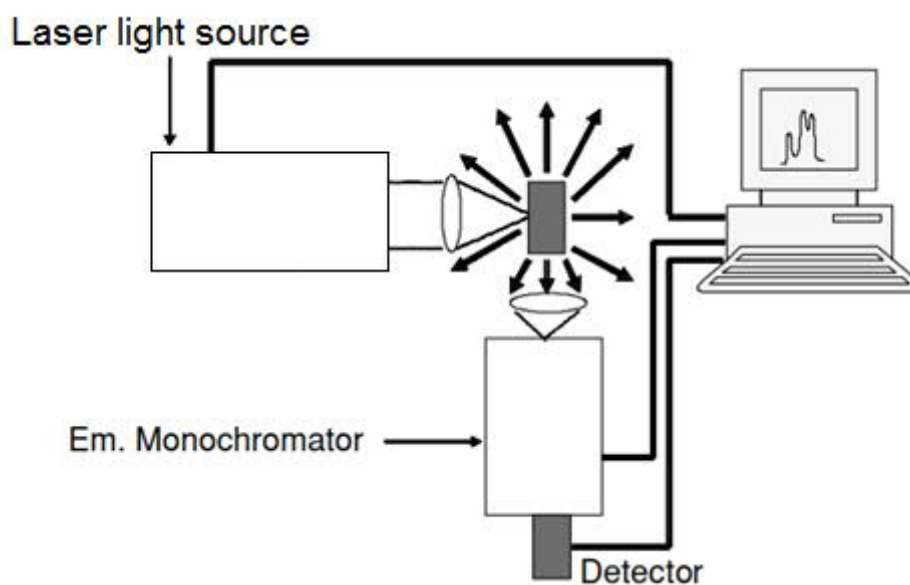
Figure 25. Schematic diagram of spectrofluorometer used. Adapted from [19, p.18]

A laser diode emits a laser beam at 980 nm, hitting the sample. Some of the light is absorbed and emitted at other wavelengths. The emitted light is then passed to a spectrometer (Instrument Systems Spectro 320 - 131). The emission spectrum is then recorded. The emission was measured from 1400 nm to 1700 nm at 0.5nm intervals. Upconversion was measured from 350 nm to 860 nm at 0.5 nm intervals.

3.6 Raman spectra measurement

The Raman spectra were measured with a very similar setup to one used in emission measurements. A high power laser light beam hits the sample and the scattered light is analyzed. Instead of using emitted light, scattered light spectra is measured. The incidient laser source light scattered and reflected from the sample is filtered off with a long-pass filter and the Stokes shifted light is recorded with a spectrometer. The peaks in Raman spectra correspond to structural bonds and therefore give us information on the materials structure.

The Raman spectra was measured with an inVia™ Qontor® confocal Raman microscope, using a 405 or 532 nm laser, 2400lpmm grating and a 50x objective. The spectra was recorded from 400 to 1500 cm^{-1}.

3.7 XRD

The crystalline materials were studied using x-ray diffraction (XRD). In XRD, a collimated beam of x-rays is scattered at various angles relative to the sample surface. When the crystal lattice spacing is a multiple of x-ray wavelength, x-rays are reflected to the sensor. The method relies on constructive interference, reflected from crystal planes acting as Bragg mirrors. When the crystal planes reflect x-ray at different angles of incidence, we can observe the crystal structure or lack of from the reflected signal.[35]

The XRD spectra were measured on PANalytic EMPYREAN, using a Cu tube with acceleration voltage of 45 kV and current of 40mA. The samples were powdered by hand with a mortar and pestle. The patterns were collected from the powdered samples placed on a "zero-background" holder

3.8 SEM/EDS

Scanning electron microscope (SEM) (Leo 1530 Gemini, Zeiss) was used to image the glasses and to study the glass and particle composition in co-operation energy dispersive x-ray spectroscopy (EDS) (Oxford Instruments X-ACT). In a SEM, a stream of electrons in accelerated and collimated into a beam, which impacts a sample. Electrons and reflecting from the sample are collected to a detector, producing an image. Advantage of SEM is that it does not require light to function and therefore is not diffraction limited, enabling higher resolution. [36, p.21-25] A schematic diagram of an SEM is shown in Figure 26.
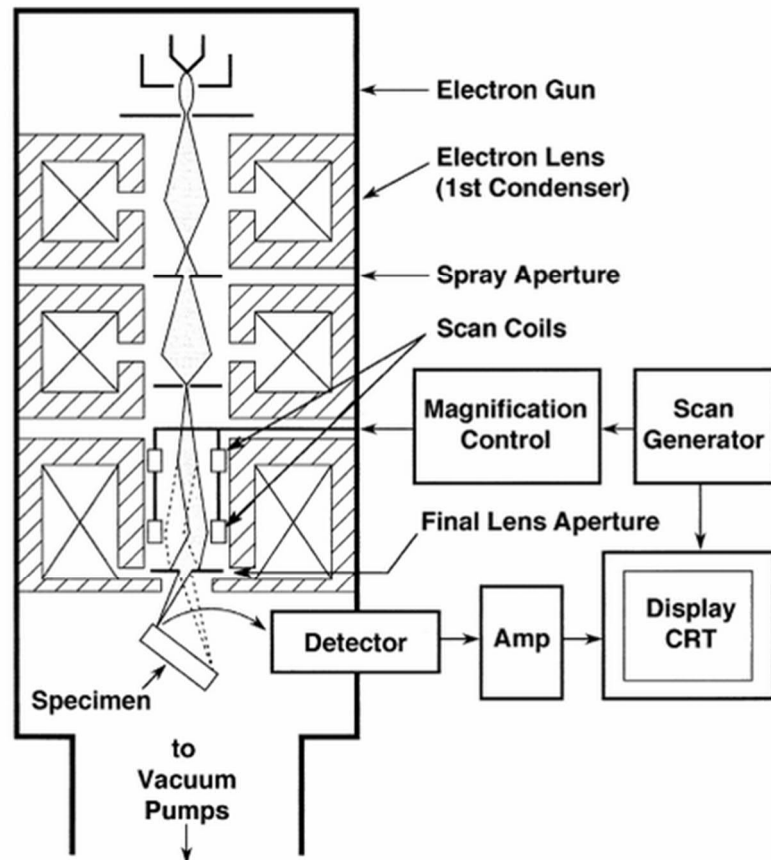
Figure 26. *Schematic diagram of a scanning electron microscope.[36, p.23]*

Attached to a SEM, an EDS can measure the spectra of x-rays that are generated when the electrons are decelerated by the sample. These x-rays have element specific energies and therefore can be used to measure the presence and amount of certain elements in samples. [36, p.297-302

4. RESULTS AND DISCUSSION

The glasses were obtained by adding the particles in the glass batch prior to the melting and in the glass melt after the melting. A mixture of the glass powder with the particles was also sintered using a hot press. We compare not only the intensity and the shape of the emission but also the homogeneity of the emission within the samples in order to determine which technique should be used in order to prepare a particles containing glass with strong emission from the particles, which are homogeneously distributed within the bulk.

4.1 Hot uniaxial pressing optimization

4.1.1 Optimizing time, temperature, pressure

The process of preparing glasses by sintering powdered glasses is not a well-established technology,and therefore the process of obtaining a clear glass had to be optimized; sintering temperature, pressure and duration needed to be optimized.

The glass with the composition (90 $NaPO_3$ - 10 NaF) (in mol%) was crushed into powder, which was sieved so only grains with the size of 38 µm or smaller were used for the sintering. At first, it was crucial to determine the maximum temperature the glass could be sintered without inducing crystallization. The thermal properties of the glass crushed into powder were first measured and the thermogram of the glass are shown in Figure 27.
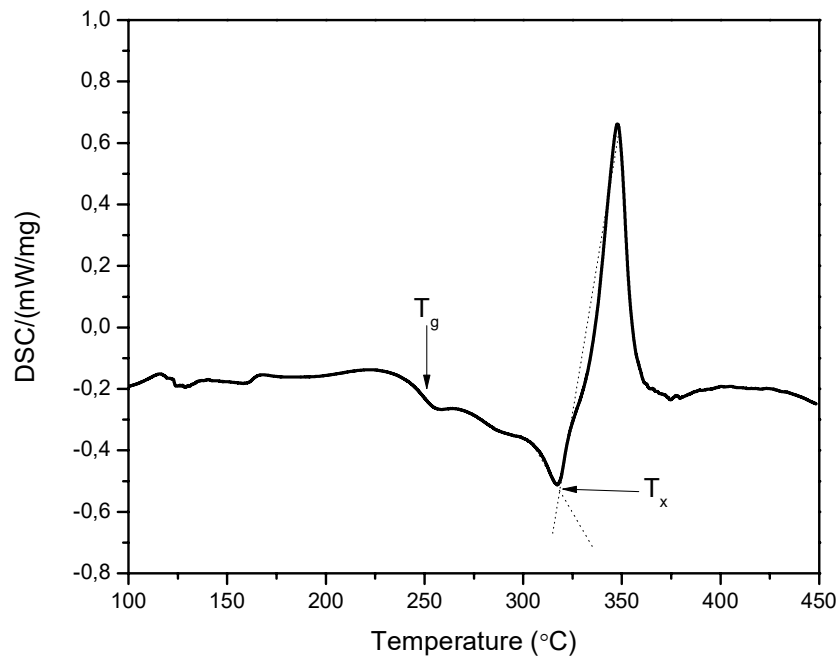
Figure 27. *Thermogram of the glass powder with T_g and T_x marked.*

The sintering temperature must be above glass transition temperature, T_g measured at 250 °C for the glass to flow viscously, but below the onset of crystallization temperature, T_x measured at 315 °C to prevent the glass from crystallizing.

Another factor in sintering performance is the glass viscosity. The viscosity curve is shown in Figure 28 [4].
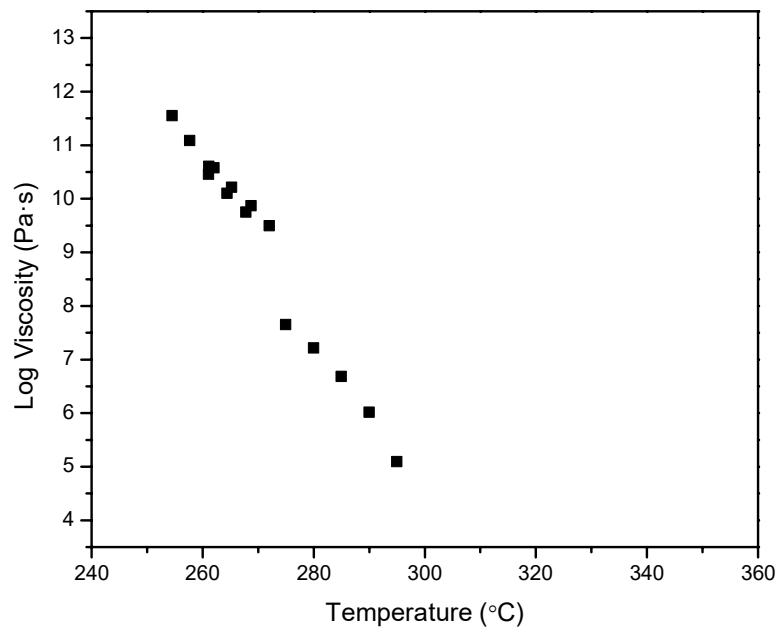
Figure 28. Viscosity of the host glass as a function of temperature. Adapted from [4]

From equation 1, the rate of densification is inversely proportional to the viscosity and therefore lower viscosities are preferred for the sintering. As per Figure 28, the Log viscosity is expected to be ~ 4.5 Pa·s at 300 °C, which was chosen as the initial temperature for sintering experiments.

As seen in Figure 29, the glass is densified but not transparent when sintered at 300°C for 30 min. The opacity of the glass is believed to come from a significant amount of pores remaining in the sintered glass indicating that pressure should be applied.
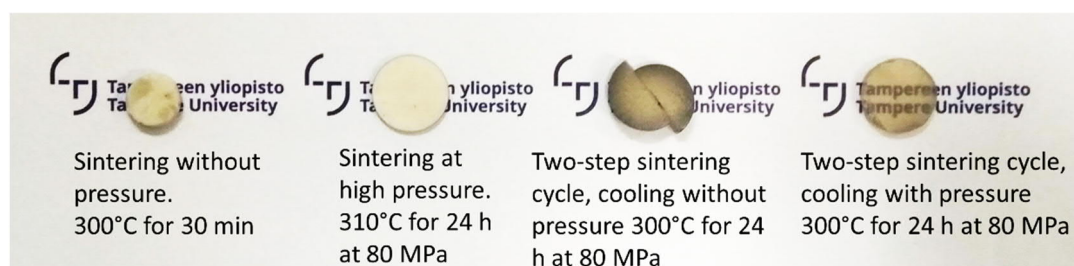
Figure 29. Various attempts towards obtaining dense and transparent sintered glass

The powder was compressed using 80 MPa pressure, which is the maximum pressure for our graphite die. While under pressure, the compact was heated at 10 °C/min to 310 °C for 24 hours and then cooled back at 5 °C/min to room temperature while under pressure. As seen in Figure 29, the glass is solid but still opaque. We believe that the high

pressure prevented initial compaction and therefore should only be used for final densi-fication. Therefore, the powder was first sintered in the die at 300 °C for 30 minutes before applying the pressure for 24 hours. At the end of this period, the pressure was removed and the temperature was decreased to room temperature. This sintering trial resulted in a broken opaque glass. The glass broke probably due to remaining stress from the experiment. Therefore, the pressure was kept at 80 MPa during the cooling period and released only after the sample had reached room temperature. As seen in Figure 29, the glass is clearly transparent with a brownish coloration.

The transmittance spectrum of the sintered glass is depicted in Figure 30.
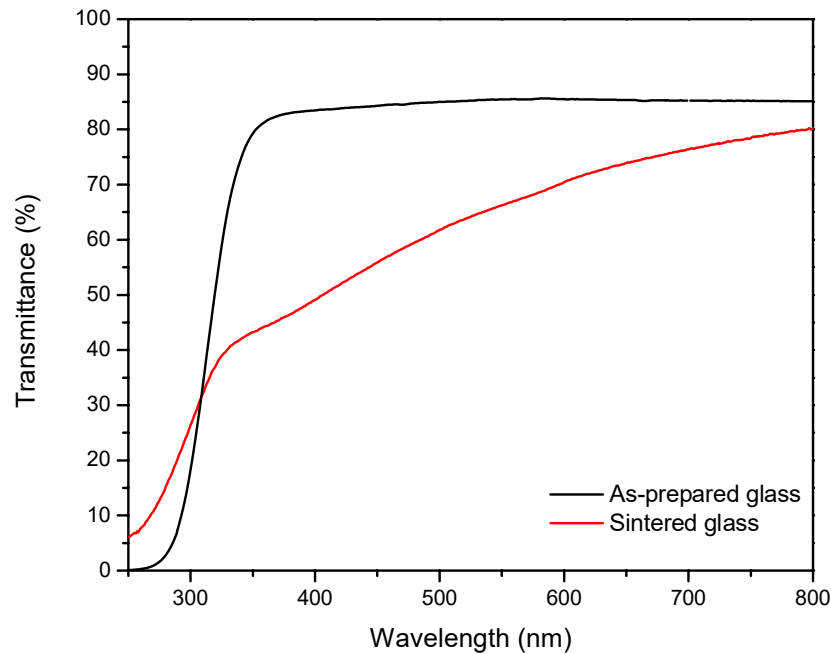
Figure 30. Transmittance of the transparent 1.5 mm thick sintered glass sample seen in Figure 29 and a 1 mm thick bulk glass sample of same composition.

As compared to the glass prepared using melting process, the transmittance of the sin-tered glass is lower. The attenuation can be explained by the scattering of small particles or defects such as pores, as Mie scattering is proportional to the inverse wavelength to the power of four, meaning that shortest wavelengths are scattered very effectively. Ad-ditionally, the brown coloration may result from carbon contamination from the mold and therefore we think that the shift of the optical band gap into the UV when comparing the transmittance spectra of the glasses may be attributed to carbon inclusion to the net-work[37]. Attempts were made to limit the carbon contamination by placing aluminum foil between the powder and the die but the resulting sintered exhibits the similar brown coloration.

Figure 31 shows microscope images at 5x and 20x magnifications. Non-sintered particles can be seen in the glass after polishing. These particles have dimensions ranging from original sieve size of 38 µm down to single micrometer range. As Mie scattering becomes noticeable at dimensions on the order of the wavelength, we can therefore assume that Mie scattering is at least in part responsible for the brown coloration present.
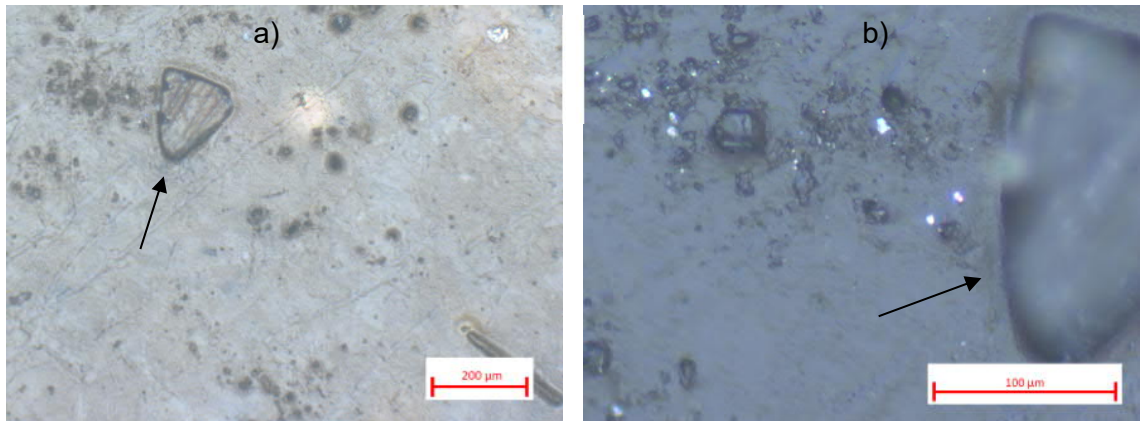
Figure 31. *Microscope images of the sintered clear glass, taken at 5x (a) and 20x (b) magnification. Arrows showing the presence of unsintered particles*

The Raman spectra of the glass prior to and after sintered are shown in Figure 32.
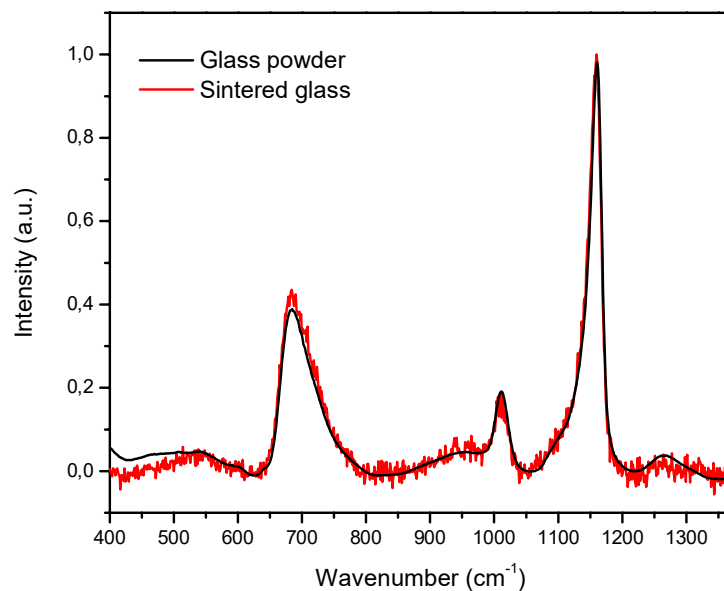
Figure 32. *Raman spectra of the transparent sintered glass and of the as-prepared glass*

The Raman spectra exhibit different bands, which can be attributed to Q^1 and Q^2 phosphate units indicating that the glass has a metaphosphate structure. The band at 700 cm^{-1} can be associated with symmetric stretching modes of *P–O–P* bridges (*v_s(P-O-P)*).

The shoulder at 950 cm^{-1} can be related to asymmetric PO$_4$ stretch on Q^0 tetrahedrons and the band at 1000 and 1140 cm^{-1} to symmetrical and asymmetrical stretching modes of Q^1. The Q^2 units can be evidenced by the presence of the bands at 1165 ($v_s(Q^2)$) and 1270 cm^{-1} ($v_{as}(Q^2)$). [12, 38] Shape and the position of the bands do not vary after sintering indicating that no significant changes to the internal glass structure occur during sintering. The presence of the carbon was also checked using Raman spectroscopy as carbon has a Raman band at 1350 cm^{-1} according to [39]. However, no peak can be seen at 1350 cm^{-1} indicating the glass possesses no or low amount of carbon.

Figure 33 shows a SEM image taken at the surface of the transparent sintered glass after polishing.
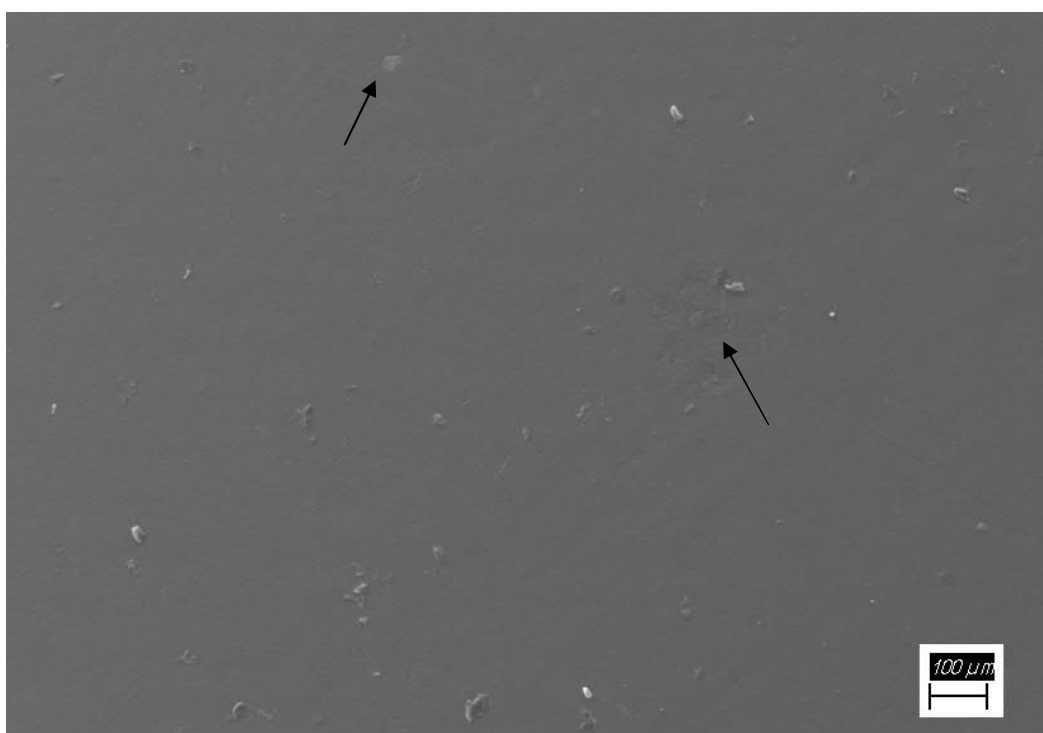
Figure 33. *SEM image of the transparent sintered glass. Arrows indicating unsintered particles.*

Figure 33 shows fairly homogeneous surface with some unsintered particles at the surface of the glass, indicated by black arrows. Detection of unsintered particles is difficult sue to very low contrast. The composition of the glass was checked using EDS. The composition of the glass is as targeted and homogeneous in the glass. According to the composition analysis, no significant loss of fluorine during melting occurred.

4.1.2 Persistent luminescent particles

As explained in [7], the glass melt has a corrosive behavior on the particles, which degrade in the glass leading to changes in the site of the rare-earth located in the particles. Therefore, it is crucial to check the impact of the sintering on the survival of the particles.

As performed in [7], the persistent luminescent (PeL) $SrAl_2O_4$ microparticles were added (0.5 wt%) in the glass powder prior to sintering. These particles were chosen as it is easy to track the decomposition of the particles through the changes in their persistent luminescence. The mixture was sintered using the optimized sintered parameters. For reference, pure particles were also sintered into a loose compact using the same process parameters.

As seen in Figure 34a, the sintered glass is transparent and still exhibits the brown coloration.
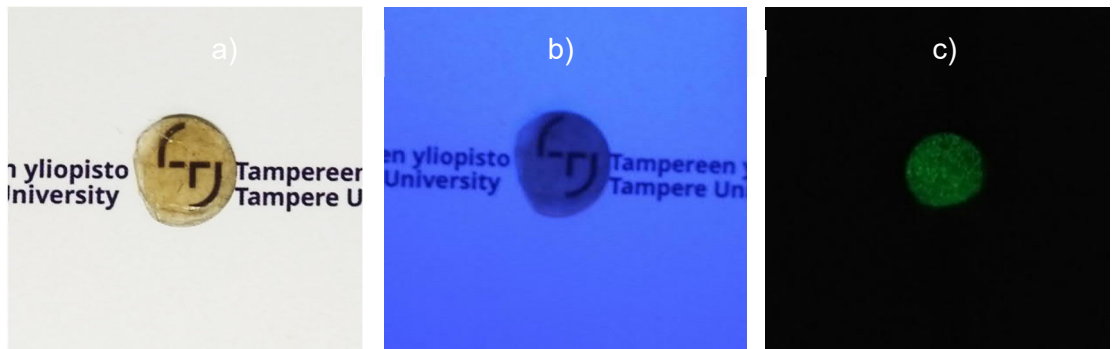
Figure 34. Glass containing persistent luminescent particles under normal illumination (a), under UV illumination (b), without external illumination after UV (c).

After stopping the UV light, the glass exhibits green PeL confirming the survival of the particles. Compared to the other PeL glasses prepared in the group [40], the PeL distribution is homogeneous.

To check if the sintering process has an impact on the site of Eu^{2+}, the persistent and conventional emission spectra were measured. They are shown below in Figure 35.
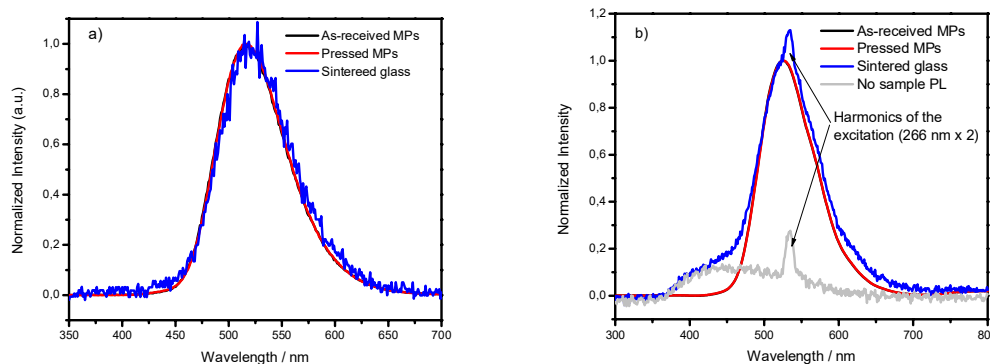
Figure 35. *Persistent (a) and conventional (b) emission spectra of the sintered glass and of the particles alone. The PeL measurements were performed by illuminating the samples with 4 W UV lamp at 254 nm for 5 minutes. Emission spectra were recorded 1 minute after stopping the illumination. Conventional emission spectra were measured using a 266 nm laser.*

The PeL spectrum of the sintered glass exhibits the same broad band at ~520 nm than the particles alone. This band can be attributed to the $4f^6 5d^1 \rightarrow 4f^7$ emission from Eu^{2+}.[41] The conventional luminescence spectrum of the sintered glass exhibits a single broad band at 525nm with a shoulder at 420 nm which is not visible in the PeL spectra of the particles alone. The band at 525nm can be associated also to the $4f^6 5d^1 \rightarrow 4f^7$ emission from Eu^{2+}. The shoulder at 420 nm was also detected when measuring the excitation. This signal is most probably the emission from the filter between the sample/holder and the detector: the more excitation is reflected from the sample, the stronger this signal is. Nonetheless, it is clearly shown that the sintered glass exhibits similar emissions band than the particles confirming that there is no change in the Er^{2+} site. We can therefore assume that the sintering process does not affect the particles' structure. As the emission bands are symmetric, Eu^{2+} are suspected to be located in one site in the particles.

The spectra also show the harmonics of the excitation source which can be explained by the samples' reflective properties. The glass reflections go predominantly in few angles whereas for the powders, the reflections are more omnidirectional because of the random orientations of the particles. The powder samples reflect only a small portion of the excitation from the sample towards the detector.

4.2   Preparation of active particles in glass

4.2.1 Overview of glasses

Figure 36 shows the picture of the particles containing glasses which were prepared using melting process and also using sintering. The wt% denotes the mass of the added particles.
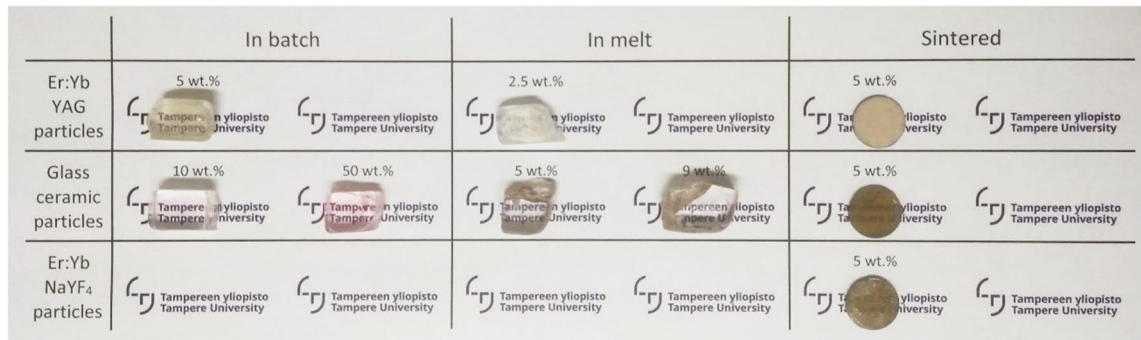
Figure 36. *Picture of the different particles containing glasses prepared using the melting and sintering processes.*

YAG containing glasses: the glass was prepared by adding 5 wt% of particles into the batch and the melt. The glasses are transparent, but cloudy, indicating that the YAG particles agglomerated during the glass melting limiting their dispersion in the glass. However, the amount of particles was too high for the dispersion of the particles in the glass melt. A large amount of particles remained at the surface of the melt. Therefore, the concentration of YAG particles was reduced to 2.5 wt% in order to improve the particle distribution within the glass during the direct doping process. Agglomerates of particles can be seen in the glasses confirming the survival of the particles.

5 wt% of the particles was used for the hot-press sintering technique. As compared to the undoped sintered glass, the sintered glass with the particles is not transparent. The opacity of the glass can be related to the presence of the YAG particles, which scatter the light. The amount of the YAG particles may be too high and/or the particles too large for the sintering of transparent glass. One should point out that the refractive index of YAG is high, ~1.8[42], compared to the ~1.5 for the host glass[43]. According to Figure 14, the particles and their agglomerates should not exceed 100 nm in size in order to prepare transparent glass containing YAG particles. As seen in Figure 37, white spots can be seen in the sintered glass. These white spots are presumably YAG agglomerates. We can therefore assume that the YAG particles are agglomerated resulting in opaque bulk due to also the high refractive index contrast.
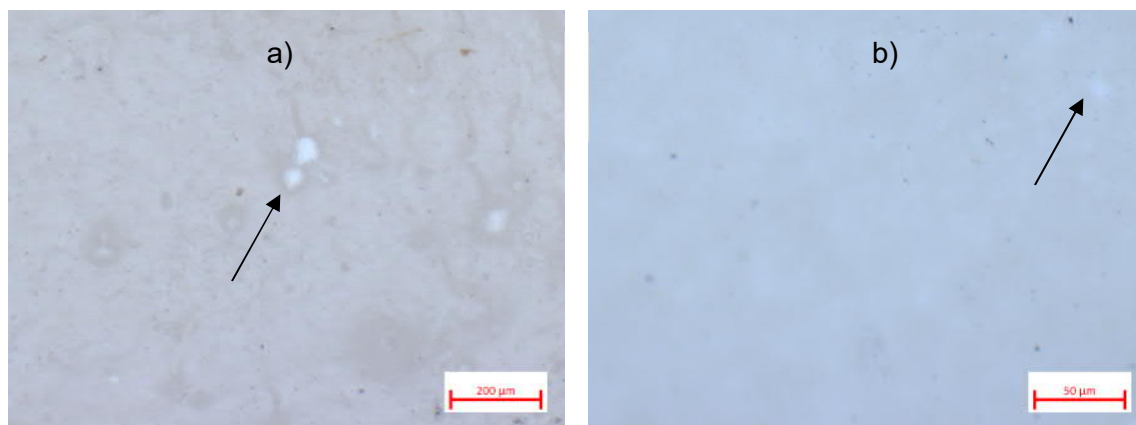
Figure 37. *Microscope images of the sintered glass containing 5 wt% of YAG. Black arrows indicate YAG agglomerates.*

GC-containing glasses: the glasses were first prepared by adding 10 wt% of GC powder into the batch and melt. It was found that when added to the melt, the particles appeared to decompose and dissolve into the melt as suspected from the pink coloration of the glass. To counteract this, a sample with 50 wt% GC particles was prepared. Both glasses are transparent with no apparent agglomerates of particles. Both of the glasses are pink, the glass with the largest amount of GC particles being the most pink. As for the YAG containing glasses, it was not possible to add 10 wt% of GC particles in the melt as the particles remain at the surface of the glass melt. Therefore, glasses were prepared with 5 and 9 wt% of GCs, and the batch size was increased from 6 to 10 grams. The increase in batch size was intended to increase the thermal inertia and so to ease the doping process. Larger batches would cool down less rapidly during the doping process and therefore would retain lower viscosity allowing a better diffusion of the particles. The sintered glass is transparent and exhibits the same brown coloration seen in the undoped sintered glass. Particle inclusions are well dispersed in the glass and could be seen in Figure 38.
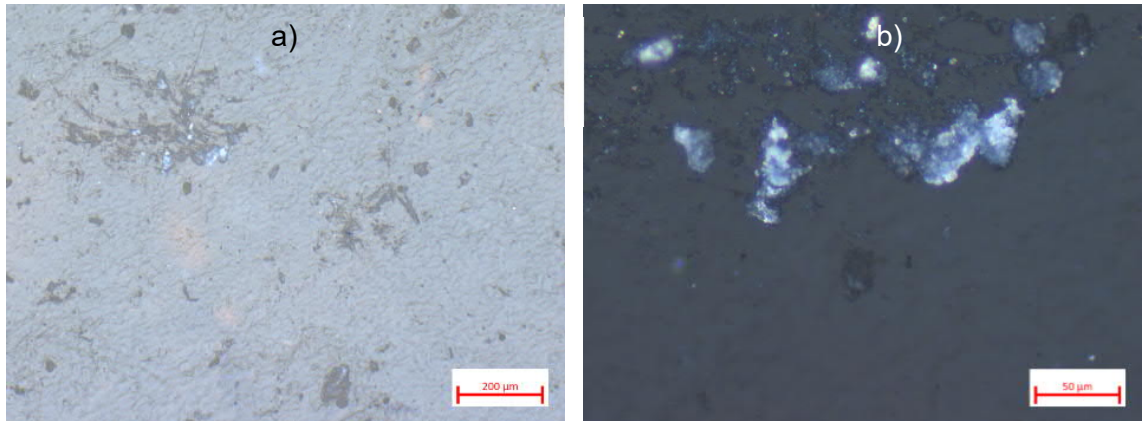
Figure 38. Microscope images of the sintered glass containing 5 wt% of GC.

Since the GCs and host glass powders had roughly the same size, we cannot differentiate the two different materials based on size. The pictures in Figure 38 just show that the sintering process was incomplete and not all particles fused together. From SEM and EDS measurements we could verify that some particles remain in glass.

NaYF₄ containing glasses: as for the sintered GC containing glass, the sintered glass is transparent and exhibits the same brown coloration. We can clearly see below in Figure 39 the agglomeration of the nanoparticles into very large agglomerates, over 100 µm in diameter. These particles are in fact so large that the largest ones can be seen with the naked eye.
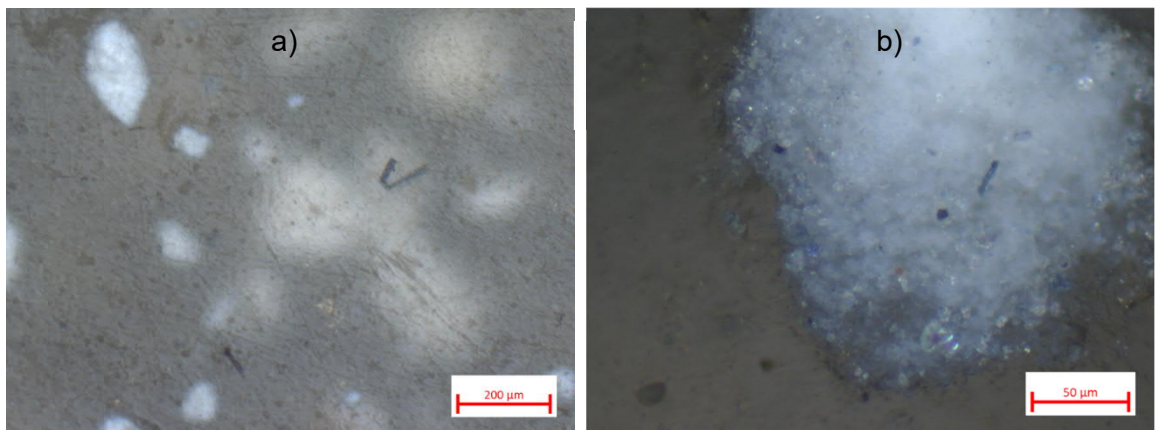
Figure 39. Microscope images of the sintered glass containing 5 wt% NaYF₄ nanoparticles.

Table 2. The density of the glasses (g cm^{-3}), accurate to ±0.02 g cm^{-3}

	In batch		In melt		Sintering	
YAG	5 wt.%	2.60	2.5 wt.%	2.51	5 wt.%	2.58
GC	10 wt.%	2.55	5 wt.%	2.53	5 wt.%	2.53
	50 wt.%	2.63	9 wt.%	2.54		
NaYF$_4$	-		-		5 wt.%	2.56

The densities of the glasses are summarized in Table 2. The density of the particles containing glasses is larger than the density of the undoped sintered glass (2.53±0.02) g/cm^3 confirming the presence of the particles in the glasses. However, one can notice that the density of the glasses prepared by adding the YAG particles in the melt is smaller than the density of the other glasses indicating that the particles might not be all dispersed in the glasses. Therefore, we expect the YAG 'in melt' glass to be less concentrated in the particles. The glasses prepared by adding the particles in the batch have similar density than the sintered glasses when prepared with similar amount of particles.

4.2.2 YAG containing glasses

In order to confirm the survival of the YAG particles, the XRD patterns of the glasses were measured. They are shown in Figure 40.
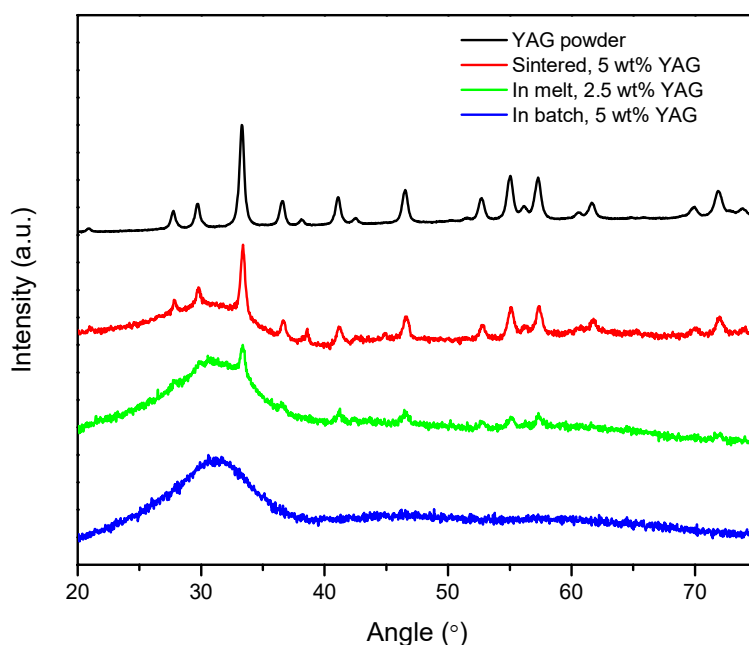
Figure 40. *XRD spectra of the YAG particles and YAG containing glasses.*

The XRD pattern of the YAG particles exhibit peaks which can be seen in the XRD pattern of the glass, prepared by adding the particles in the glass melt and in the pattern of the sintered glass confirming the survival of the YAG particles in these glasses. The difference in the peak intensity between the XRD patterns is related to the different amount of YAG particles in the glasses. However, the glass prepared by adding the particles in the batch does not exhibit sharp peak although particles can be seen by naked eyes. The amount of the particles is probably too low to be detected and/or the dispersion of the particles is inhomogeneous.

The emission spectra at 1.5µm of the glasses are presented in Figure 41. The spectra were measured in different areas in order to check the changes in the intensity of the emission within the bulk.
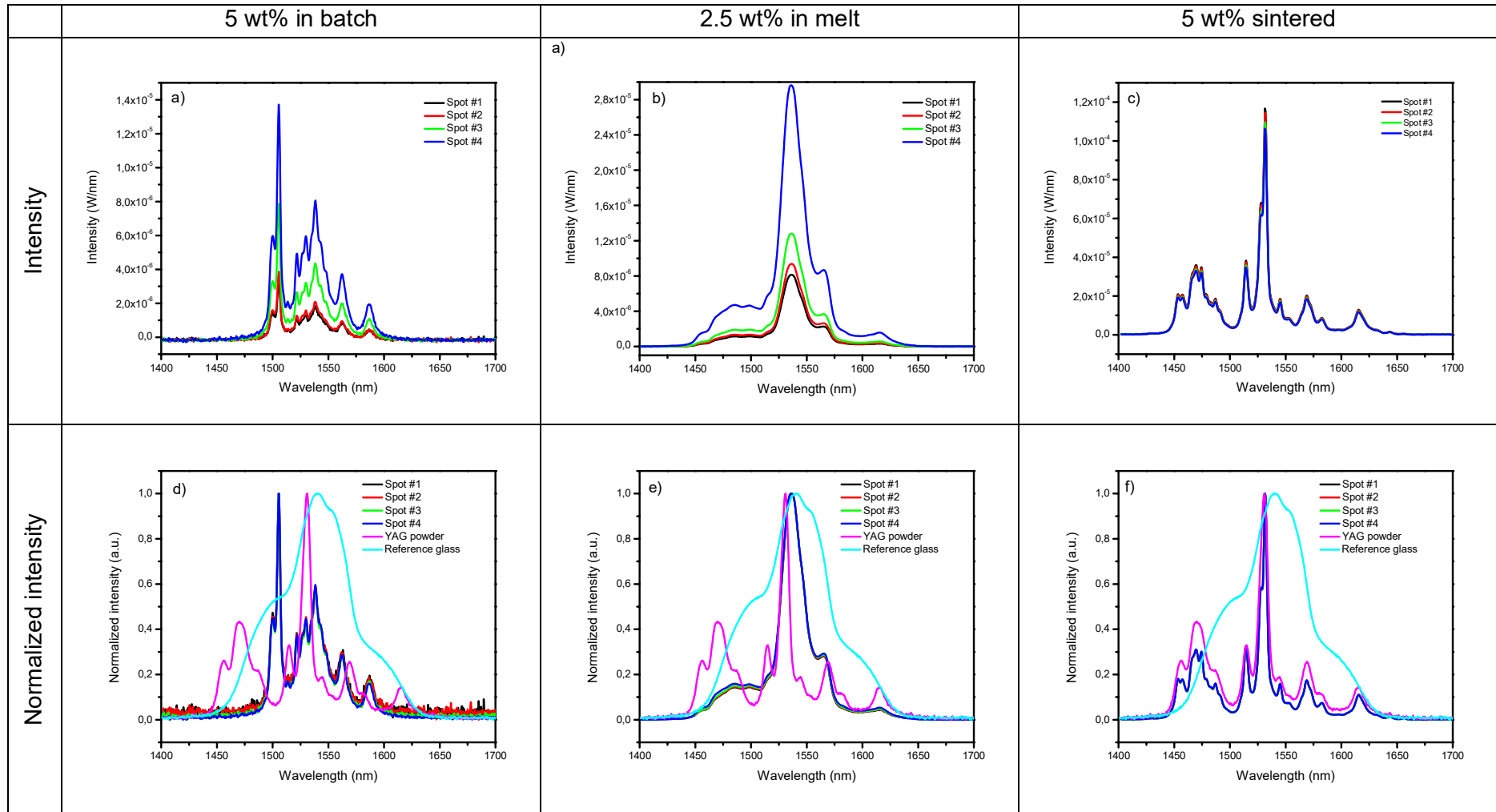
Figure 41. *Intensity and normalized intensity of emission band at 1550 nm of the YAG containing glasses (excitation at 980 nm).*

After pumping at 980nm, all glasses exhibit an emission in the 1400- 1700nm range, which is due to the $^4I_{13/2} \rightarrow {}^4I_{15/2}$ transition of Er^{3+}. [44]

The intensity of the emission varies significantly in the glasses prepared when adding the YAG particles into the batch and in the melt indicating that the particles are not well distributed in the glasses (Figure 41a and b). This is in agreement with the agglomerates visible to the naked eye. The intensity of emission in the sintered glass seen in Figure 41c is nearly identical across the surface indicating a homogenous distribution of particles in the glass. One can notice that the emission from this glass is 10 times stronger than in the other glasses. Therefore, we expect that a larger amount of YAG particles survived during the sintering process than during the melting process.

No variation in the shape of the emission can be seen within the different areas in all the samples. However, one can notice that the shape of the emission depends on the fabrication method. The emission band exhibits sharp peaks when adding the particles in the batch (Figure 41d) while broad bands are detected from the glasses prepared by adding the particles in the melt (Figure 41e). Both the bands are different than the emission band of the YAG particles. These changes are a clear sign of changes in the Er^{3+} site and are a result of the corrosive melt as suggested in previous research[4]. Due to the presence of peaks in the emission band, we expect the Er^{3+} ions to be located in crystalline site in the 'in melt' glass. One can notice that the shape of the emission is different than the emission of the glass doped with Er^{3+} prepared using a standard melting process indicating that Al and Y might enter the site of the Er^{3+} in amorphous glass due to the decomposition of the particles during preparation of the glass. It is important to mention that the sintered glass exhibits similar emission band than the YAG powder (Figure 41f), indicating that minimal changes in the Er^{3+} site occurred during the sintering process and so confirming the survival of the YAG particles.

The upconversion spectra of the glasses are presented in Figure 42.

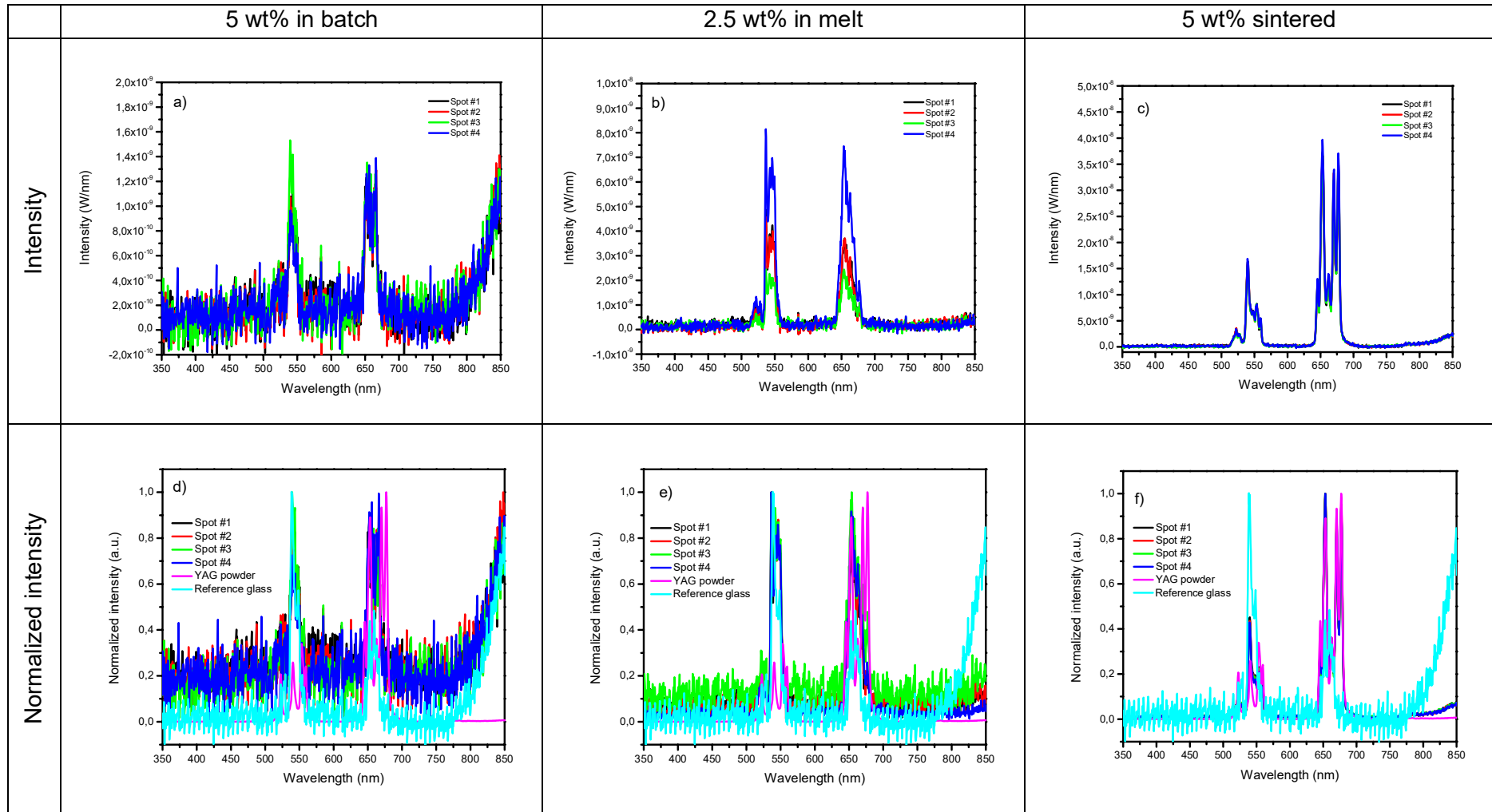***Figure 42.*** *Upconversion and normalized upconversion intensity spectra of the YAG containing glasses (excitation at 980 nm).*

The spectra exhibit several bands with bands at 520, 540 and 650 nm that are due to the transitions from $^4H_{11/2}$, $^4S_{3/2}$ and $^4F_{9/2}$ levels to ground level of Er^{3+}, respectively. [44]

As for the emission at 1.5µm, the intensity of the upconversion depends on the fabrication process, the sintered glass exhibiting the strongest intensity (Figure 42c). The glass prepared by adding the particles in the batch (Figure 42a) and in melt (Figure 42b) exhibit some upconversion, but their intensities are lower despite similar doping levels confirming that a small fraction of the YAG particles survive the melting process. Due to the lower intensity of the upconversion, a lower amount of YAG particles are suspected to survive the melting process when added in the glass batch than when added in the glass melt, which is in agreement with the XRD results. The sintered glass is the only sample with homogeneous intensity of upconversion. The sintered glass has emission almost identical to the powdered YAG, again confirming little or no changes in the site of Er^{3+} during the preparation of the glass.

4.2.3 GC particles containing glasses

GC particles containing glasses were prepared by adding the particles in the glass melt. However, as seen in Figure 43, agglomerate of GC particles can be seen in the glasses
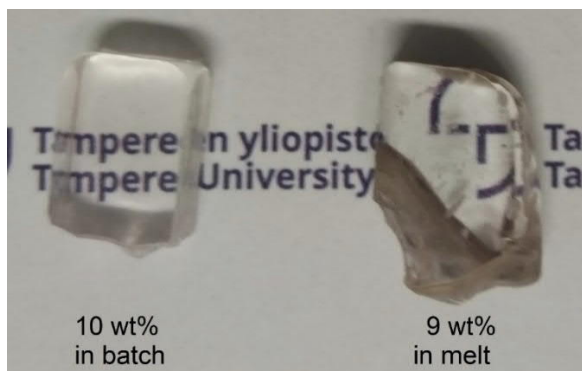
Figure 43. Picture of 'in batch' and 'in melt' -glasses.

As a reminder, these GC particles are from a heat-treated glass crushed into particles with a size of 38 µm, which is probably too large. In order to prepare a transparent glass, the size of the particles should be reduced. This could be achieved by etching the particles using phosphoric acid [45].

The first step was to determine the etching rate. GC cubes of 5 mm in size were immersed in phosphoric acid and the glass was weighted as a function of immersion time. From mass loss, the linear etch distance was calculated. The results for 1M phosphoric acid solution are shown in Figure 44.
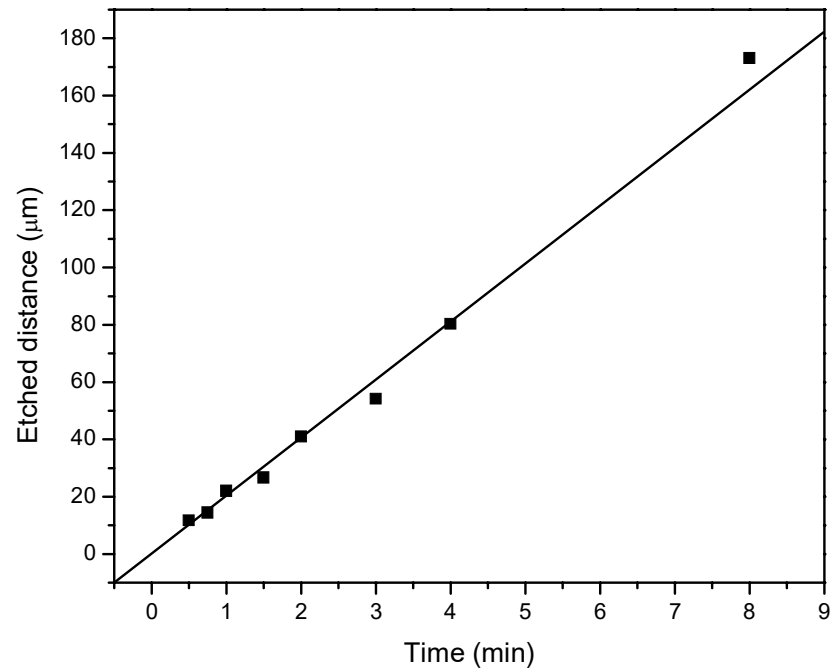
Figure 44. *GC etch rate in 1M phosphoric acid.*

Figure 44 shows linear trend giving an etching rate of 20.9 µm/min. The etching of the GC powder was attempted. However, etching of the powder turned out to be impossible as the powder agglomerated very aggressively and fused together. As a result, this avenue of research was discontinued and a decision was made to attempt sintering with smallest particles available. The question and possibility of chemically fusing glass particles together remains as an open question available for future research.

The XRD pattern of the glasses are shown in Figure 45.
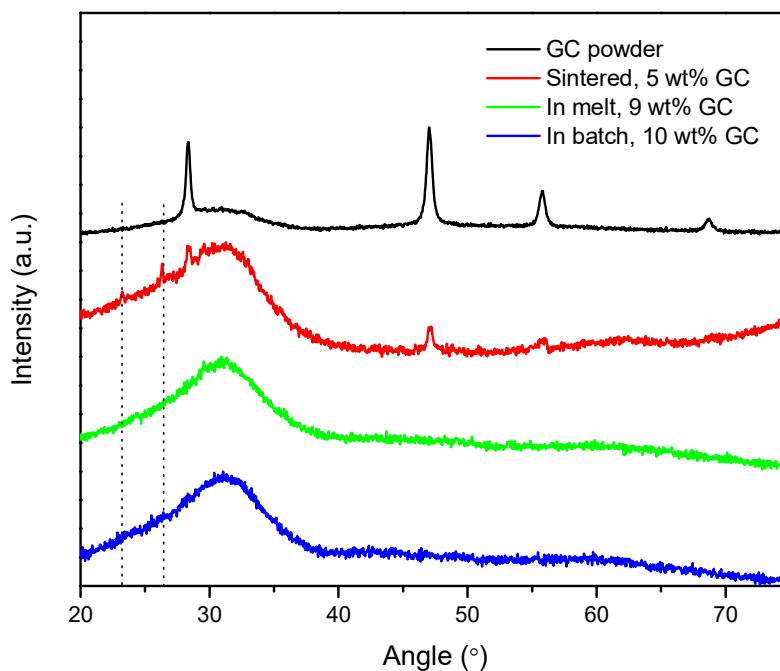
Figure 45. *XRD spectra of YAG containing glasses along with the powder spectra.*

The GCs alone exhibit few peaks which are related to CaF_2 crystals[31]. The XRD pattern of the glasses prepared using the melting process exhibit no sharp peak while the sintered glass exhibits the peaks related to CaF_2. As the sintered glass contains the lowest amount of GCs while exhibiting sharp peaks, it is possible to think that the CaF_2 did not survive the melting process when added in the batch. This was expected as some glasses have a homogenous pink coloration. As clumps can be seen in the glass prepared by adding the particles in the melt, we think that the absence of XRD peaks can be related to an inhomogeneous distribution of particles in the glass.

One can notice that the XRD pattern of the sintered glass exhibit additional peaks at around 23° and 26°, marked with dotted lines. These peaks likely belong to crystalline $NaPO_3$ (ICDD PDF# 00-011-0648). As these peaks are not present in the GC powder spectrum, we must assume that the sintering process has induced some crystallization in the host glass powder.

The transmittance spectrum of the sintered glass is shown in Figure 46

Figure 46. *Transmittance of 1 mm thick sample of as-prepared glass, 1.5 mm thick sintered glass and a 1.4 mm thick sample glass containing 5 wt% of GC. Erbium absorptions shown with arrows.*

The transmittance of the GCs containing glass is lower than the transmittance of the undoped sintered glass. We think it is the presence of GCs particles, the carbon contamination and the residual pores which increase the scattering and attenuation. The transmittance spectra of the p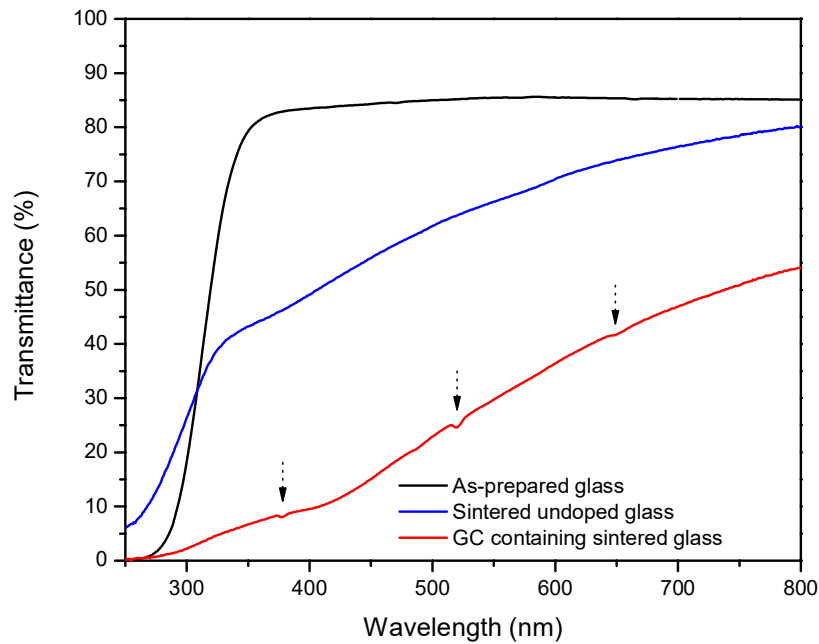articles containing sintered glass exhibit the absorption of Er^{3+} ions at 380 nm, 540 nm and 650 nm corresponding to transitions from $^4I_{15/2}$ ground level to $^4G_{9/2}$ + $^4G_{11/2}$ level, $^4S_{3/2}$, and $^4F_{9/2}$ levels respectively. [44]

The emission spectra of the glasses prepared by adding the particles in the batch are shown in Figure 47. Although the glasses look homogeneous, the emission intensity varies greatly across the sample, indicating inhomogeneity in the dispersion of the GCs in the glass. The glass prepared with 10 wt% of GCs exhibits a broad emission band which is typical of Er^{3+} in glass. This band is different from the emission band of GCs alone. When the amount of the GCs increases to 50 wt %, the shape of the emission changes: the intensity of the shoulder at 1550 nm increases. The changes in the shape of the emission is a clear indication that the GC particles do not survive the melting process. As for the YAG containing glasses, the site of Er^{3+} is suspected to contain calcium in vicinity of the optical center, as one of the element of the GCs because the shape of the emission of Er^{3+} is different than the emission of Er^{3+} in the glass prepared using standard melting process.
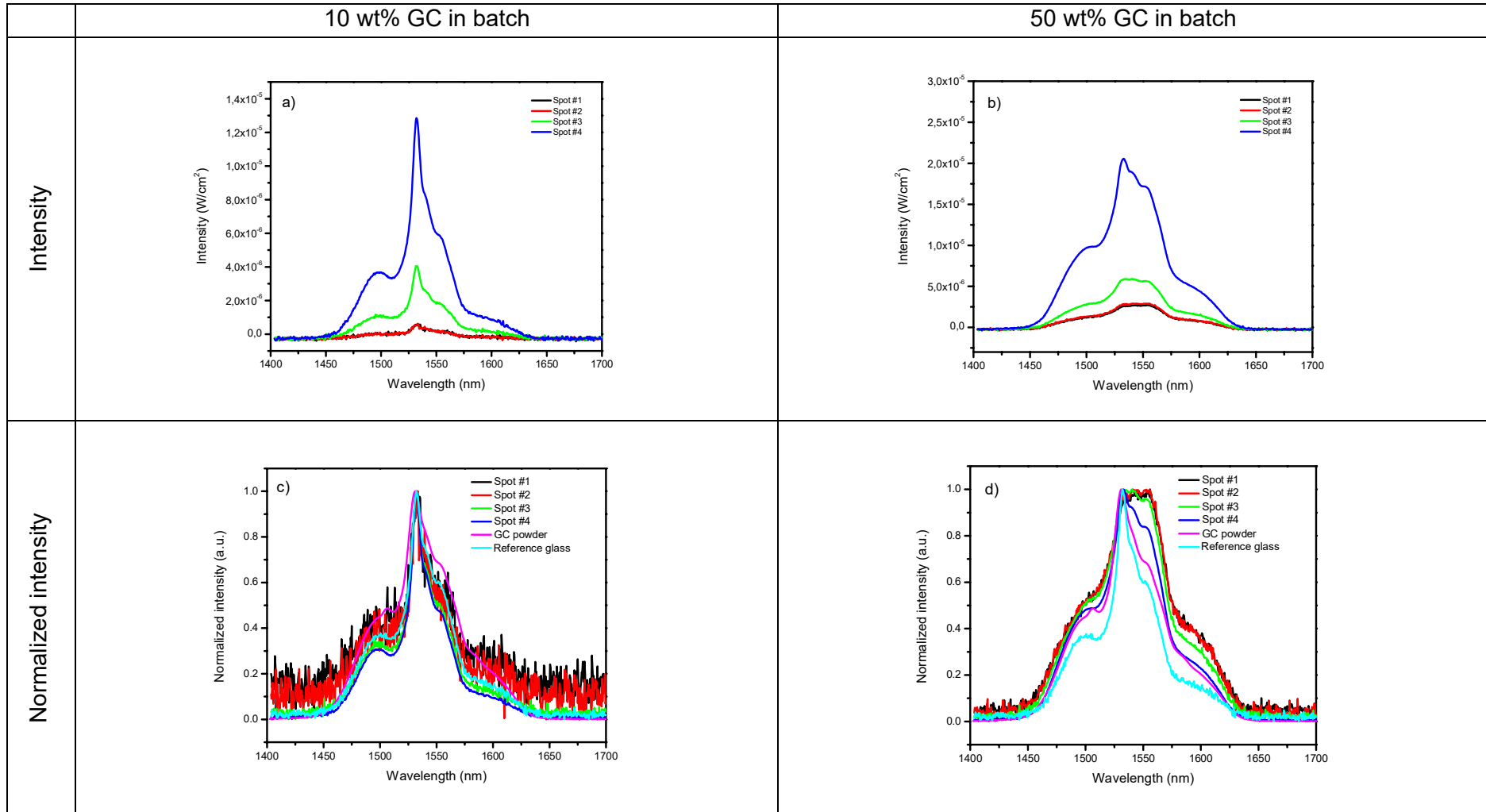
Figure 47. *Intensity and normalized intensity of emission band at 1.5µm for GC 'in batch' –glasses (excitation at 980 nm).*
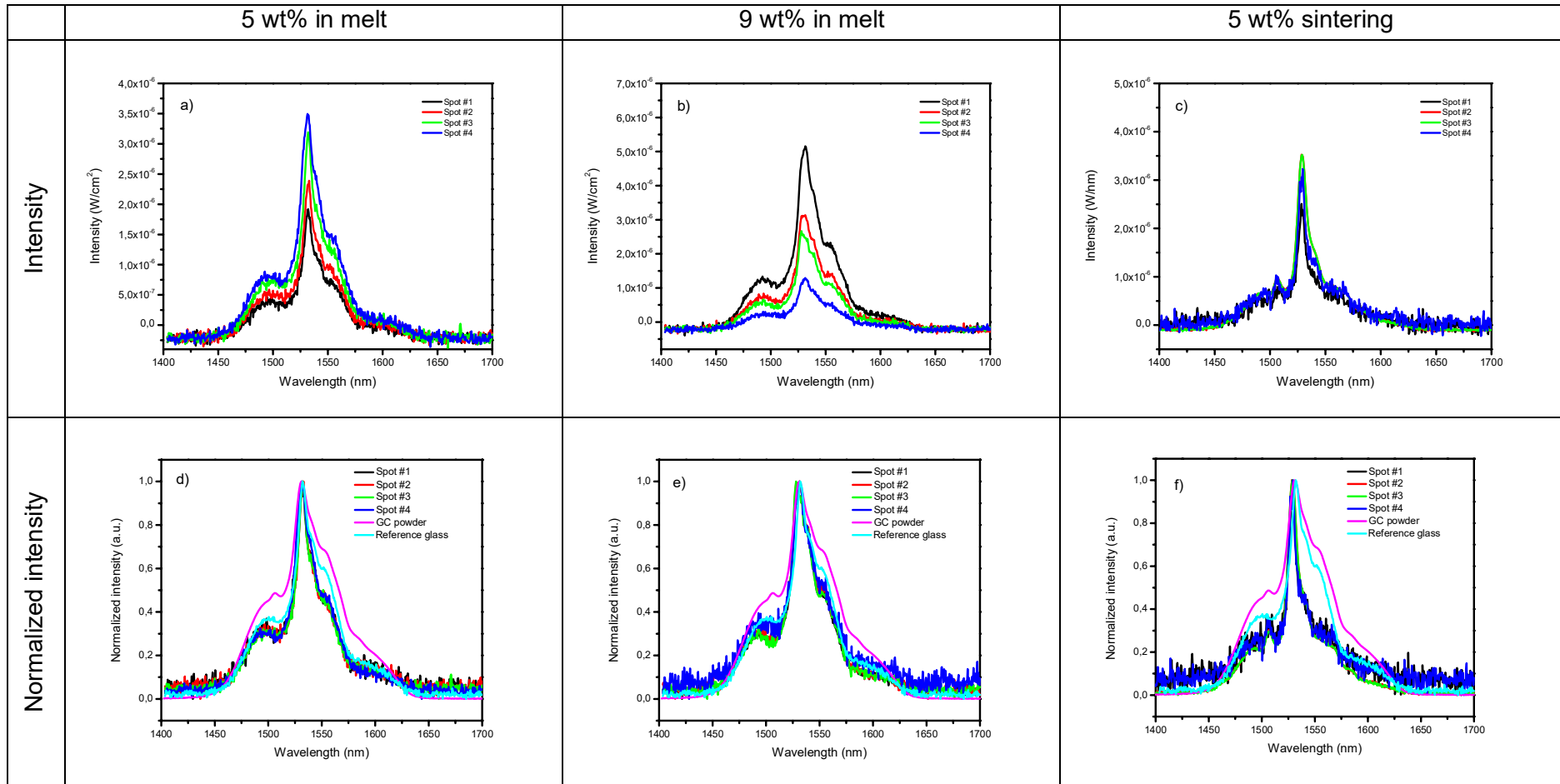
Figure 48. *Intensity and normalized intensity of emission band at 1.5 µm for GC sintered and 'in melt' –glasses (excitation at 980 nm).*

The emission spectra of the other glasses are depicted in Figure 48. The emission varies when measured in different locations in the glasses prepared via the direct doping method (Figure 48a and b). This is evidence that the particles, and the erbium dissolving from them, are not well dispersed in the glass. The glasses exhibit similar shape (Figure 48d and e) which is also similar to the emission from the glass prepared by adding the GC particles in the melt, indicating together with XRD data that the GC particles mostly dissolved into the glass during manufacturing of the glass using the melting processes. The emission of the sintered glass is very homogeneous, as seen in Figure 48c. Surprisingly, the emission peak is very narrow compared to the signal of the GC particles alone indicating that the sintering has an impact on the site of Er^{3+} and so on the GC particles.

The upconversion spectra of the glasses are shown in Figure 49 and Figure 50. All the glasses exhibit the green and red emissions from Er^{3+} after 980 nm pumping. The intensity of the upconversion in the glasses prepared by the melting process seems to be related to the amount of particles. All the glasses exhibit different upconversion than the particles alone confirming that the preparation of the glass has an impact on the GCs. The addition of the GCs in the glass is not fully understood and should be investigated deeper.

	10 wt% GC in batch	50 wt% GC in batch
Intensity		
Normalized intensity		
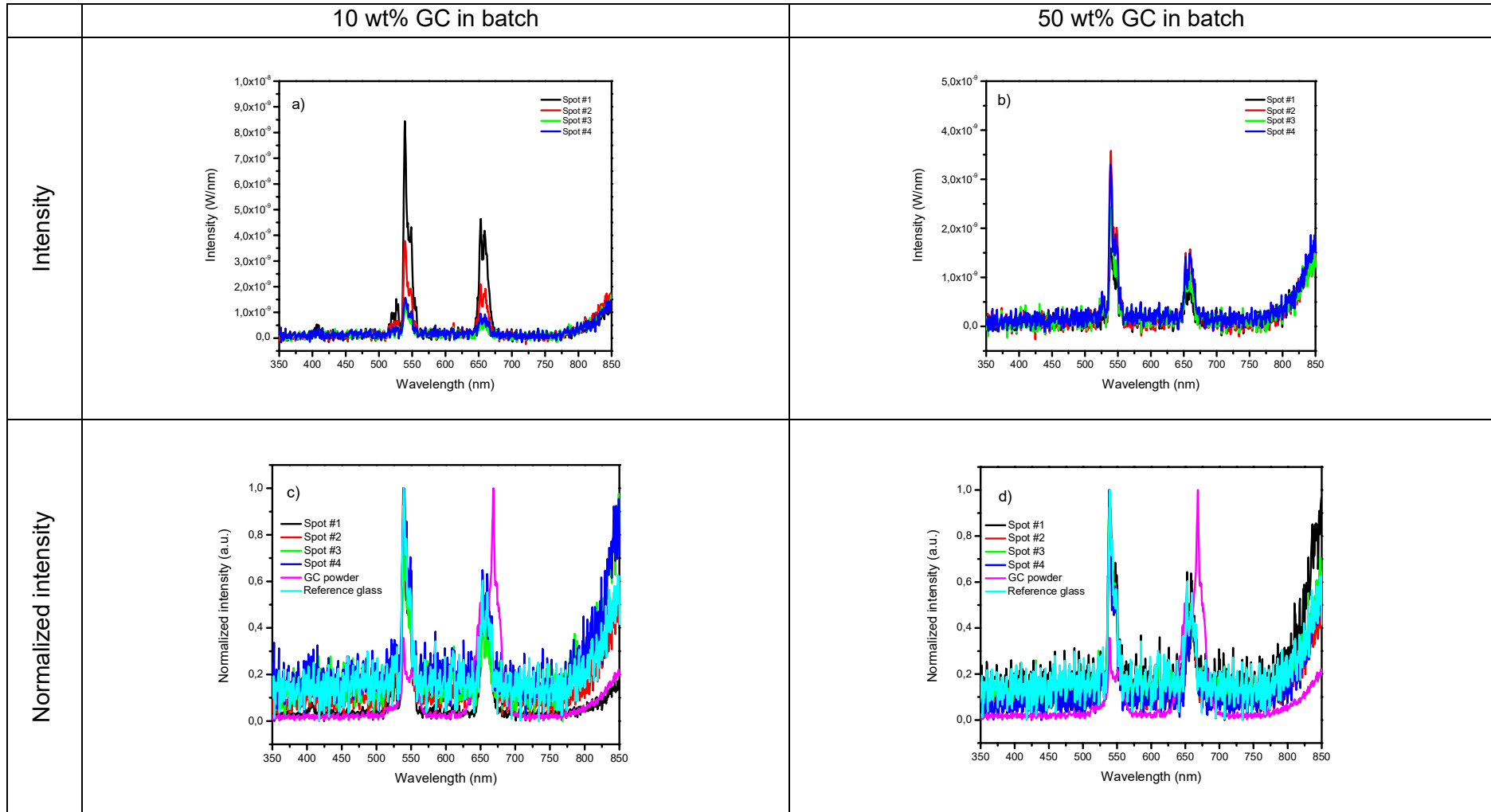
Figure 49. Upconversion and normalized upconversion spectra of 'in batch' GC-containing glasses. (excitation at 980 nm).
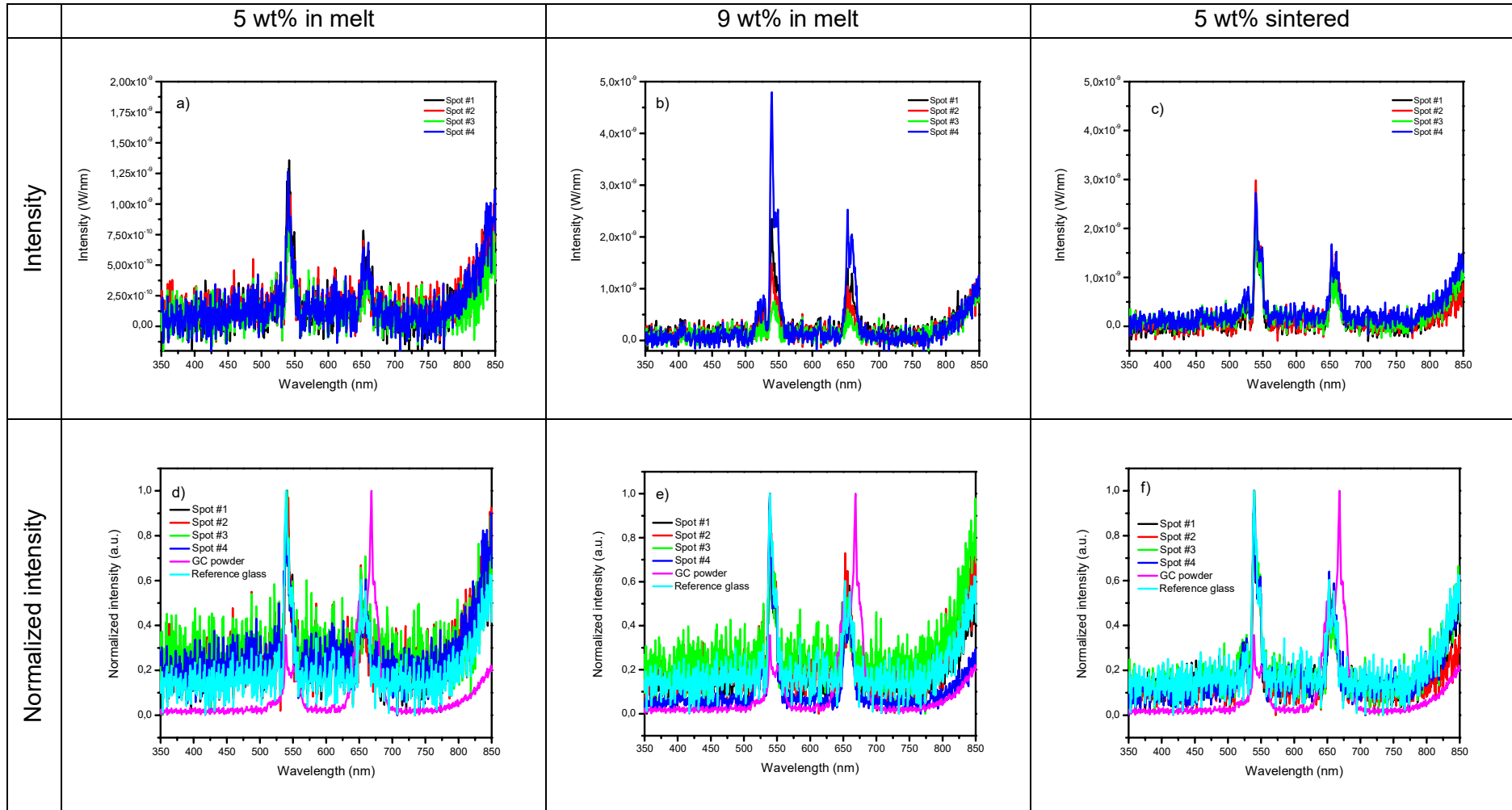
Figure 50. *Upconversion and normalized upconversion spectra of 'in melt' and sintered, GC -containing glasses (excitation at 980 nm)*

4.2.4 NaYF4 containing glasses

In a previous study [4], it was shown that the NaYF$_4$ nanoparticles fully degraded in the glass when added in the batch prior to the melting. However, these nanoparticles can be successfully added into a fluorophosphate glass system using the direct doping method if the doping parameters are controlled. As reported in [4], it is, however, difficult to pre-pare a glass with homogeneous dispersion of the particles. Therefore, we focus here on the preparation of the same glass using the sintering process. Below is shown the XRD pattern of the glass with NaYF$_4$ powder for reference.
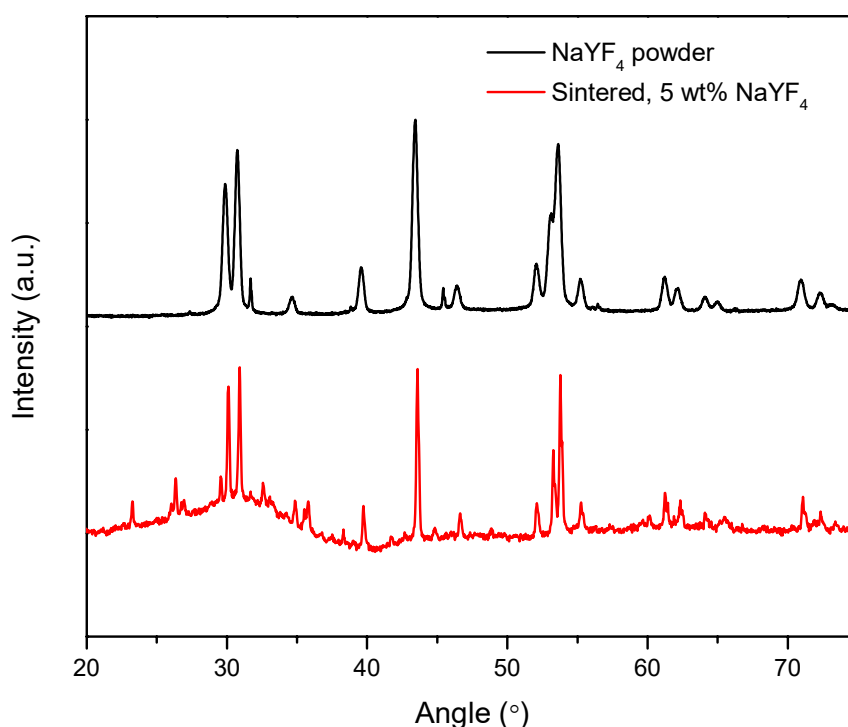
Figure 51. XRD spectra of NaYF$_4$ nanoparticles and of the sintered glass

The pattern of the sintered glass exhibits similar peaks than those seen in the XRD of the nanoparticles alone but also additional peaks which can be related to NaPO$_3$ crys-talline peaks seen also in sintered GC containing glass. The presence of NaPO$_3$ crystals was also confirmed using micro-Raman spectroscopy. The Raman spectra were meas-ured near an agglomerate of particles.
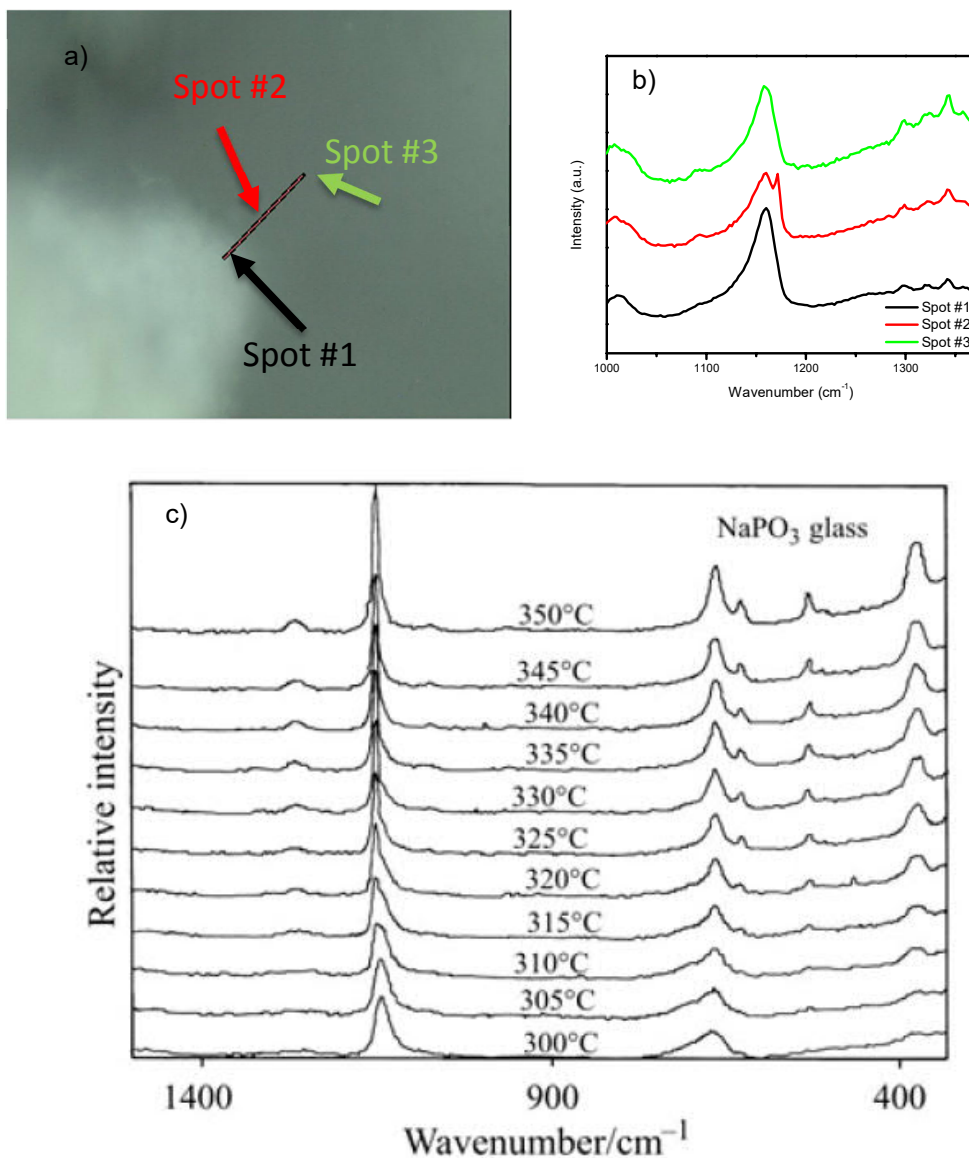
Figure 52. Micro-Raman picture (a), associated spectra (b) measured at three different locations. Excited at 405 nm. Raman spectra of the NaPO₃ glass heat treated at different temperatures [46] (c)

Figure 52c Shows that crystalline $NaPO_3$ has its main peak at around 1150 cm^{-1}, which is sharper and shifted towards larger wavenumbers than in case of amorphous $NaPO_3$. The Raman spectra in Figure 52b exhibit similar peaks than those presented in Figure 52c. The peak at 1150 cm^{-1}, which according to [46], can be related to crystalline $NaPO_3$. This peak is visible only in the spectrum collected at the glass-particle interface indicating that the host glass undergoes crystallization at the particle and glass interface. The transmittance of the glass is presented in Figure 53.
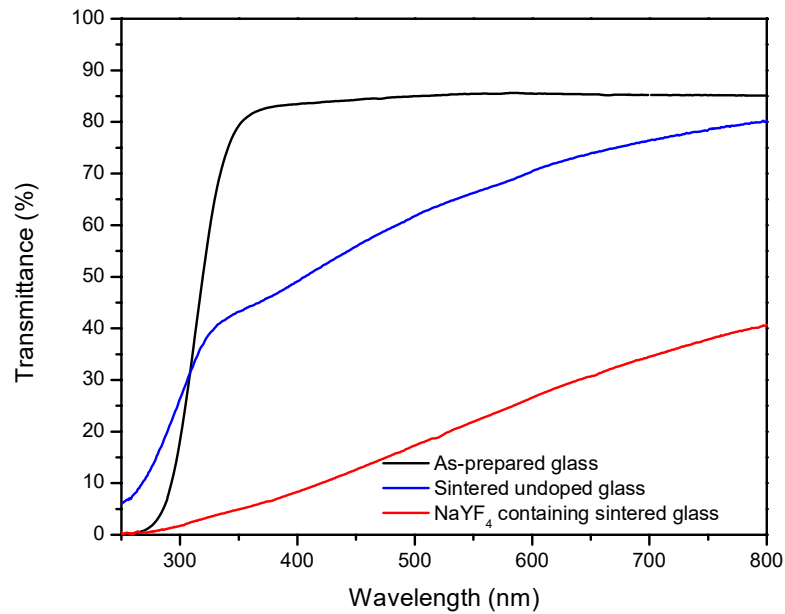
Figure 53. *Transmittance of a 1 mm thick sample of as -prepared glass, 1.5 mm thick sintered glass and a 1.4 mm thick sample of glass containing 5 wt% of NaYF$_4$*

As seen for the other sintered glass, the addition of the particles decreases the transmittance of the glass. The emission at 1.5 µm and the upconversion spectra of the glasses are depicted in Figure 54. The intensity of emission from the sintered glass varies slightly with the location but within the 10% accuracy of the measurement, one can consider that there is no variation in the emission at 1.5µm and in the visible within the sample (Figure 54a and b). The shape of the emission at 1.5µm and in the visible (Figure 54c and d) are very similar than that of the particles alone confirming that the sintering process has no significant impact on the NaYF$_4$ nanoparticles.

.
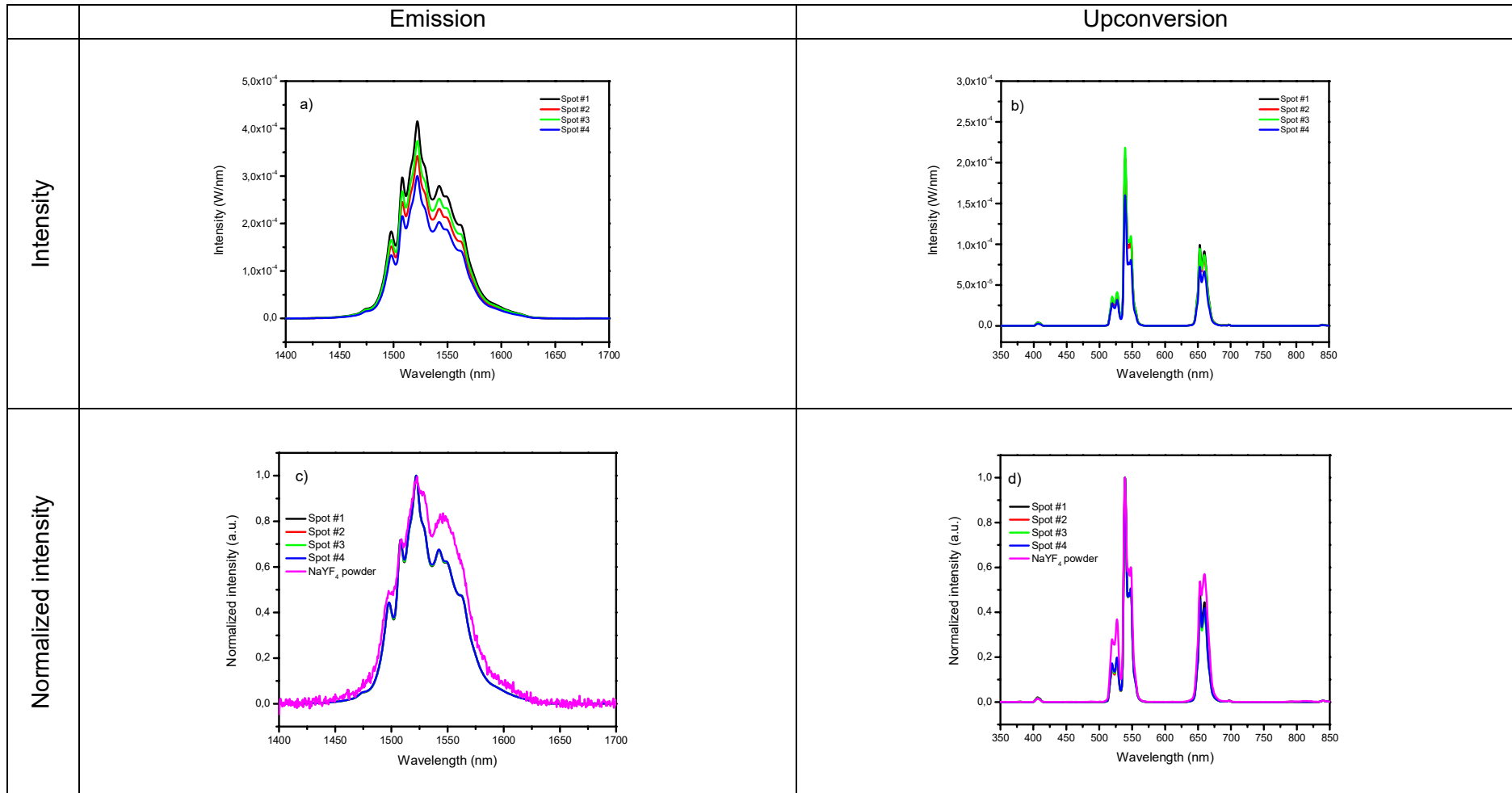
Figure 54. *Intensity and normalized intensity of emission at 1.5µm and upconversion spectra for sintered glass containing 5 wt% of NaYF₄ particles and NaYF₄ particles (excitation at 980 nm)*

5. CONCLUSIONS

In this thesis, different particles containing phosphate glasses were prepared using direct doping and sintering processes. The particles were YAG and $NaYF_4$ co-doped with Yb^{3+} and Er^{3+}. An Er^{3+} doped glass with the composition ($75NaPO_3$-$25CaF_2$) (in mol%) was heat treated in order to form a transparent glass-ceramic with CaF_2 crystals doped with Er^{3+} dispersed in the volume of the glass. This glass-ceramic was crushed into powder. In the melting process, the particles were added in the glass batch and in the glass melt. Additionally, they were mixed with powdered host glass prior to sintering the mixtures.

A method of preparing transparent glass by hot uniaxial pressing from powdered glass was studied in detail. The sintering parameters were optimized based on sintering physics, literature, and experiments. A glass with a composition of $90\ NaPO_3$ - $10\ NaF$ (in mol%) was prepared using the standard melting method, crushed into powder and sintered back into transparent glass, albeit with a brown tint. Source of this coloration could not be confirmed, but it is most likely due to the scattering from nanoscale defects and/or carbon inclusion. Once transparent glass was obtained, persistent luminescent (PeL) particles were added in the glass prior to sintering. These particles were used to gauge the suitability of this process for the preparation of particle-doped glasses and to check the survival of the particles during the sintering process. The resulting glass was transparent. The glass also exhibit strong and homogenous persistent luminescence, which is a clear indication of the survival of the particles and their homogenous distribution in the glass. Most importantly, the shape of emission from the particles containing glass was identical than that of the particles alone indicating that the sintering process has no corrosion impact on the particles.

Glasses were prepared with YAG particles using the direct doping and sintering processes. XRD data as well as the spectroscopic properties of the glasses show that the YAG particles partially survive during the direct doping procedure (both added in the batch and in the melt) and when sintered. However, the shape of the emission band changed when preparing the glass using the melting processes indicating changes in the site of the Er^{3+} in the YAG crystal after embedding the particles in the glass. The distribution of particles in the glasses prepared using melting process was inhomogene-

ous, resulting in uneven emission intensity in different spots. At the same time the emission shape of the sintered glass was similar than the emission shape of the YAG alone and particle distribution was homogeneous. The sintered samples also demonstrate the highest emission intensity.

The GC particles did not survive the melting or direct doping processes and dissolved in the molten glass or remained at the surface of the melt without dispersing in the glass melt. The emission bands were similar to the emission band of a glass doped with Er^{3+} ions indicating that the Er^{3+} in the particles containing glass are probably located in an amorphous site. However, the sintered glass exhibit narrow emission band indicating that Er^{3+} are located in a crystal. However, the shape of the emission is different than that of the GC alone suggesting that the sintering process leads to changes in the Er^{3+} site. One should point out that $NaPO_3$ crystals were found to precipitate during sintering.

The $NaYF_4$ particles in sintered glass were heavily agglomerated as evident from microscope images. The emissions bands were unaffected by sintering process. Formation of crystalline $NaPO_3$ was also seen in the XRD pattern of the glass and further confirmed using Raman spectroscopy.

To conclude, with this study, we show the sintering process holds great promise. The hot-pressing procedure reveals to be more gentle and less corrosive procedure, which results in less particles degradation and high crystallinity of the glass-ceramics, when compared to the direct doping technique. It is demonstrated, that the sintering technique is capable to produce transparent glass-ceramic materials, activated by RE-doped crystals. This, however, requires thorough optimization of the sintering process and was not achieved for all the particles considered in this work. It is important to note, that current experiments were limited by mechanical limits of the graphite die, which doesn't allow to use pressures above 80 MPa. Use of a metal die would allow to use higher pressures and temperatures and could enable better sintering performance resulting in clearer glass-ceramics. Moreover a better die will allow to test other glass systems, use shorter cycle times during sintering as well as eliminate possible source of carbon contamination. Special care must be taken to prevent crystallization during sintering. The study should be focused on understanding how glasses respond to long periods under pressure at temperatures close to the onset of crystallization. It is also crucial to check if the active particles induce the crystallization during the sintering process, mechanisms of the particles degradation. Finally, the failed attempt in particle size reduction left an interesting question on whether glass particles could be fused together chemically. This would represent an entirely new avenue of research.

REFERENCES

[1] M. Yamane, Y. Asahara, Glasses for Photonics by Masayuki Yamane, Cambridge University Press, 2000, 284 p.

[2] H. Nguyen, M. Tuomisto, J. Oksa, T. Salminen, M. Lastusaari, L. Petit, Upconversion in low rare-earth concentrated phosphate glasses using direct NaYF4:Er3+, Yb3+ nanoparticles doping, Scripta Materialia, Vol. 139, 2017, pp. 130-133.

[3] J. Massera, M. Gaussiran, P. Głuchowski, M. Lastusaari, L. Petit, J. Hölsä, L. Hupa, Effect of the glass melting condition on the processing of phosphate-based glass–ceramics with persistent luminescence properties, Optical Materials, Vol. 52, 2016, pp. 56-61.

[4] N. Ojha, M. Tuomisto, M. Lastusaari, L. Petit, Upconversion from fluorophosphate glasses prepared with NaYF4:Er3+,Yb3+ nanocrystals, RSC Advances, Vol. 8, Iss. 34, 2018, pp. 19226-19236.

[5] Q. Pan, Z. Cai, Y. Yang, D. Yang, S. Kang, Z. Chen, J. Qiu, Q. Zhan, G. Dong, Engineering Tunable Broadband Near-Infrared Emission in Transparent Rare-Earth Doped Nanocrystals-in-Glass Composites via a Bottom-Up Strategy, Advanced Optical Materials, Vol. 7, Iss. 6, 2019, pp. 1801482.

[6] J. Zhao, X. Zheng, E.P. Schartner, P. Ionescu, R. Zhang, T. Nguyen, D. Jin, H. Ebendorff-Heidepriem, Upconversion Nanocrystal-Doped Glass: A New Paradigm for Photonic Materials, Advanced Optical Materials, Vol. 4, Iss. 10, 2016, pp. 1507-1517.

[7] N. Ojha, H. Nguyen, T. Laihinen, T. Salminen, M. Lastusaari, L. Petit, Decomposition of persistent luminescent microparticles in corrosive phosphate glass melt, Corrosion science, Vol. 135, 2018, pp. 207-214.

[8] S. Kudo, A. Kishioka, H. Kuwahara, H. Kuroe, H.T. Hintzen, K. Itatani, Encapsulation of nitride phosphors into sintered phosphate glass by pressureless firing and hot isostatic pressing, Journal of the American Ceramic Society, Vol. 102, Iss. 3, 2019, pp. 1259-1268.

[9] W. H. Zachariasen, THE ATOMIC ARRANGEMENT IN GLASS, in: J. Am. Chem. Soc., American Chemical Society, 1932, pp. 3841-3851.

[10] J.E. Shelby, M. Lopes, Introduction to Glass Science and Technology, The Royal Society of Chemistry, 2005, 312 p.

[11] Benjah-bmm27, Silicate double tetrahedra, Wikimedia Commons, 2007, website, Available (accessed on 28.8.2019): https://commons.wikimedia.org/wiki/File:Silicate-double-tetrahedra-2D.png

[12] R.K. Brow, Review: the structure of simple phosphate glasses, Journal of Non-Crystalline Solids, Vol. 263, 2000, pp. 1-28.

[13] B.E.A. Saleh, Fundamentals of photonics, Wiley, 1991, 937-947 p.

[14] Offnfopt, Simple Periodic Table Chart, Wikimedia Commons, 2017, website, Available (accessed on 28.8.2019): https://commons.wikimedia.org/wiki/File:Simple_Periodic_Table_Chart-en.svg

[15] M.J. Weber, Science and technology of laser glass, Journal of Non-Crystalline Solids, Vol. 123, Iss. 1, 1990, pp. 208-222.

[16] A.J Kenyon, Recent developments in rare-earth doped materials for optoelectronics, in: Progress in Quantum Electronics, Elsevier Ltd, 2002, pp. 225-284.

[17] C.I. Oppo, R. Corpino, P.C. Ricci, M.C. Paul, S. Das, M. Pal, S.K. Bhadra, S. Yoo, M.P. Kalita, A.J. Boyland, J.K. Sahu, P. Ghigna, F. d'Acapito, Incorporation of Yb3+ ions in multicomponent phase-separated fibre glass preforms, Optical materials, Vol. 34, Iss. 4, 1992, pp. 660-664.

[18] D.J. Richardson, J. Nilsson, W.A. Clarkson, High power fiber lasers: current status and future perspectives, JOSA B, Vol. 27, Iss. 11, 2010, pp. B6-B92.

[19] J. García Solé, L.E. Bausá, D. Jaque, An Introduction to the Optical Spectroscopy of Inorganic Solids, John Wiley & Sons, Ltd, 2005, .

[20] E. Hecht, Optics, Addison-Wesley, 2002, 698 p.

[21] T. Wriedt, Mie Theory: A Review, in: W. Hergert, T. Wriedt (ed.), The Mie Theory: Basics and Applications, Springer Berlin Heidelberg, Berlin, Heidelberg, 2012, pp. 53-71.

[22] F. Auzel, D. Pecile, D. Morin, Rare Earth Doped Vitroceramics: New, Efficient, Blue and Green Emitting Materials for Infrared Up-Conversion, Journal of The Electrochemical Society, Vol. 122, Iss. 1, 1975, pp. 101-107.

[23] M.J. Dejneka, The luminescence and structure of novel transparent oxyfluoride glass-ceramics, Journal of Non-Crystalline Solids, Vol. 239, Iss. 1, 1998, pp. 149-155.

[24] S. Karthika, T.K. Radhakrishnan, P. Kalaichelvi, A Review of Classical and Non-classical Nucleation Theories, Crystal Growth & Design, Vol. 16, Iss. 11, 2016, pp. 6663-6681.

[25] P.P. Fedorov, A.A. Luginina, A.I. Popov, Journal of fluorine chemistry, Journal of fluorine chemistry, Vol. 172, 1971, pp. 22-50.

[26] K. Abe, J. Hamada, M. Miyazawa, H. Kuwahara, K. Itatani, Fabrication of transparent sintered ZnO-B2O3-Bi2O3glass body by pressureless firing and hot isostatic pressing, IOP Conference Series: Materials Science and Engineering, Vol. 47, 2013, pp. 012024.

[27] E.M. Rabinovich, Preparation of glass by sintering, Journal of Materials Science, Vol. 20, Iss. 12, 1985, pp. 4259-4297.

[28] J. Frenkel, Kinetic Theory of Liquids, Oxford University Press, 1946, 502 p.

[29] W.B. Pietenpol, Surface Tension of Molten Glass, Physics, Vol. 7, Iss. 1, 1936, pp. 26-31.

[30] T. Laihinen, M. Lastusaari, L. Pihlgren, L. Rodrigues, J. Hölsä, Thermal behaviour of the NaYF4:Yb3+,R3+ materials, Journal of Thermal Analysis and Calorimetry, Vol. 121, Iss. 1, 2015, pp. 37-43.

[31] A. Nommeots-Nomm, N.G. Boetti, T. Salminen, J. Massera, M. Hokka, L. Petit, Luminescence of Er 3+ doped oxyfluoride phosphate glasses and glass-ceramics, Journal of Alloys and Compounds, Vol. 751, 2018, pp. 224-230.

[32] P. Roldán Del Cerro, T. Salminen, M. Lastusaari, L. Petit, Scripta materialia, Scripta materialia, Vol. 151, 2018, pp. 38-41.

[33] Compact Hot Pellet Press up to 1000C with 30 Segment Temperature Control - EQ -HP-6T, MTI Corp., website, Available (accessed on 28.8.2019): http://www.mtixtl.com/CompactHotPelletPresswith30SegmentTemperatureControl-EQ-HP-6T.aspx.

[34] J. Yang, C. Roy, Using DTA to quantitatively determine enthalpy change over a wide temperature range by the "mass-difference baseline method", Thermochimica Acta, Vol. 333, Iss. 2, 1999, pp. 131-140.

[35] Y. Waseda, E. Matsubara, K. Shinoda, X-Ray Diffraction Crystallography: Introduction, Examples and Solved Problems, Springer Berlin Heidelberg, 2011, .

[36] J.I. Goldstein, D.E. Newbury, P. Echlin, D.C. Joy, C.E. Lyman, E. Lifshin, L. Sawyer, J.R. Michael, Introduction, in: J.I. Goldstein, D.E. Newbury, P. Echlin, D.C. Joy, C.E. Lyman, E. Lifshin, L. Sawyer, J.R. Michael (ed.), Scanning Electron Microscopy and X-ray Microanalysis: Third Edition, Springer US, Boston, MA, 2003, 550p.

[37] J.A. Jiménez, M. Sendova, E.R. Fachini, C. Zhao, Enhanced UV transparency in phosphate glasses via multi-wall carbon nanotubes, Journal of Materials Chemistry C, Vol. 4, Iss. 41, 2016, pp. 9771-9778.

[38] D. Möncke, H. Eckert, Review on the structural analysis of fluoride-phosphate and fluoro-phosphate glasses, Journal of Non-Crystalline Solids: X, Vol. 3, 2019, pp. 100026.

[39] A.C. Ferrari, J. Robertson, Interpretation of Raman spectra of disordered and amorphous carbon, Physical Review B, Vol. 61, Iss. 20, 2000, pp. 14095-14107.

[40] N. Ojha, T. Laihinen, T. Salminen, M. Lastusaari, L. Petit, Ceramics international, Vol. 44, Iss. 10, 1981, pp. 11807-11811.

[41] T. Aitasalo, J. Holsa, H. Jungener, J.-C. Krupa, M. Lastusaari, J. Legendziewicz, J. Niittykoski, Effect of temperature on the luminescence processes of SrAl2O4: Eu2+, Radiation Measurements, Vol. 38, 2004, pp. 727-730.

[42] D.E. Zelmon, D.L. Small, R. Page, Refractive-index measurements of undoped yttrium aluminum garnet from 0.4 to 5.0 μm, Applied Optics, Vol. 37, Iss. 21, 1998, pp. 4933-4935.

[43] S. Chaguetmi, A. Boutarfaia, M. Poulain, Physical Properties of Ternary NaPO3-KHSO4-MX (M=Na, K and X=Cl, Br) Glasses, Energy Procedia, Vol. 74, 2015, pp. 470-476.

[44] R. Yow, D. Dee, R. Debnath, K. Nash, J. Gruber, D. Sardar, Optical characterization and ligand-field splitting of Er 3 + (4 f 11) energy levels in a fluorine containing tellurite glass, Journal of

[45] P. Lopez-Iscoa, N. Ojha, D. Pugliese, A. Mishra, R. Gumenyuk, N.G. Boetti, D. Janner, J. Troles, B. Bureau, C. Boussard-Plédel, J. Massera, D. Milanese, L. Petit, Design, processing, and characterization of an optical core-bioactive clad phosphate

fiber for biomedical applications, Journal of the American Ceramic Society, Vol. 0, Iss. 0, 2019,

[46] R. Sridarane, G. Raje, D. Shanmukaraj, B. Kalaiselvi, M. Santhi, S. Subramanian, S. Mohan, B. Palanivel, R. Murugan, Investigations on temperature dependent structural evolution of NaPO3 glass, Journal of Thermal Analysis and Calorimetry, Vol. 75, Iss. 1, 2004, pp. 169-178.